

1 Volcanic SO₂ Layer Height by TROPOMI/S5P; evaluation against 2 IASI/MetOp and CALIOP/CALIPSO observations.

3 Maria-Elissavet Koukouli¹, Konstantinos Michailidis¹, Pascal Hedelt², Isabelle A. Taylor³, Antje Inness⁴,
4 Lieven Clarisse⁵, Dimitris Balis¹, Dmitry Efremenko², Diego Loyola², Roy G. Grainger³ and Christian
5 Retscher⁶

6 ¹ Laboratory of Atmospheric Physics, Aristotle University of Thessaloniki, Greece.

7 ² German Aerospace Center (DLR), Remote Sensing Technology Institute, Oberpfaffenhofen, Germany.

8 ³ COMET, Sub-department of Atmospheric, Oceanic and Planetary Physics, University of Oxford, UK.

9 ⁴ European Centre for Medium-Range Weather Forecasts (ECMWF), Reading, UK.

10 ⁵ Université Libre de Bruxelles (ULB), Spectroscopy, Quantum Chemistry and Atmospheric Remote Sensing (SQUARES),
11 Brussels, Belgium.

12 ⁶ European Space Agency, ESRI, Frascati, Rome.

13 *Corresponding author:* Hedelt, Pascal Andre, Pascal.Hedelt@dlr.de

14 **Abstract.** Volcanic eruptions eject large amounts of ash and trace gases such as sulphur dioxide (SO₂) into the atmosphere. A
15 significant difficulty in mitigating the impact of volcanic SO₂ clouds on air traffic safety is that these gas emissions can be
16 rapidly transported over long distances. The use of space-borne instruments enables the global monitoring of volcanic SO₂
17 emissions in an economical and risk-free manner. Within the European Space Agency (ESA) Sentinel-5p+ Innovation project,
18 the S5P SO₂ Layer Height (S5P+I: SO2LH) activities led to the improvements on the retrieval algorithm and generation of the
19 corresponding near-real-time S5P SO₂ LH products. These are currently operationally provided, in near-real-time, by the
20 German Aerospace Center (DLR) in the framework of the Innovative Products for Analyses of Atmospheric Composition,
21 INPULS, project. The main aim of this paper is to present its extensive verification, accomplished within the S5P+I: SO2LH
22 project, over major recent volcanic eruptions, against collocated space-born measurements from the IASI/Metop and
23 CALIOP/CALIPSO instruments, as well as assess its impact on the forecasts provided by the Copernicus Atmospheric
24 Monitoring Service, CAMS. The mean difference between S5P and IASI observations for the Raikoke 2019, the Nishinoshima
25 2020 and the La Soufrière-St Vincent, 2021 eruptive periods is $\sim 0.5 \pm 3$ km, while for the Taal 2020 eruption, a larger difference
26 was found, between 3 ± 3 and 4 ± 3 km. The comparison of the daily mean SO₂ layer heights further demonstrates the capabilities
27 of this near-real-time product, with slopes between 0.8 and 1 and correlation coefficients ranging between 0.6 and 0.8.
28 Comparisons between the S5P SO₂ LH and the CALIOP/CALIPSO ash plume revealed an expected bias at -2.5 ± 2 km,

29 considering that the injected SO₂ and ash plumes' locations do not always coincide over an eruption. Furthermore, the CAMS
30 assimilation of the S5PSO₂ LH product led to much improved model output against the non-assimilated IASI layer heights,
31 with a mean difference of 1.5±2 km, compared to the original CAMS analysis, and improved the geographical spread of the
32 Raikoke volcanic plume following the eruptive days.

33 **1 Introduction**

34 Ten years have passed since the ash cloud from the 2010 Icelandic Eyjafjallajökull volcano caused an unprecedented disruption
35 to air traffic across Europe, affecting the flight schedules of approximately 10 million passengers and resulting in nearly 2
36 billion US dollars in lost airline revenue (Bolić and Sivčev, 2011). This eruption led to increased awareness of the threat of
37 volcanic ash to air traffic in Europe, and numerous advances have taken place since then with regard to research, regulation,
38 and cooperation (Reichardt et al., 2017). Apart from the ash cloud, the volcanic sulphur dioxide (SO₂) plume is also hazardous
39 to aircraft, as it forms the corrosive sulphuric acid and can further deposit sulphates in the engines (Prata, 2009). Since the ash
40 particles will deposit faster than SO₂ after the first post-eruption hours, the two clouds typically separate in elevation, making
41 the reliable detection, dispersal and forecast of both clouds during significant explosive eruptions on a global basis equally
42 important (ICAO, 2019).

43 The disruption that the Eyjafjallajökull & Grímsvötn 2010 and 2011 eruptions had on airborne traffic has led the International
44 Civil Aviation Organization, ICAO, to change the previous zero tolerance policy on volcanic ash to establishing ash
45 concentration thresholds over Europe. Zehner et al., 2012, have translated these thresholds into specific requirements for
46 improved volcanic ash monitoring and forecasting services. These include the early detection of volcanic emissions and the
47 near real-time, NRT, global monitoring of volcanic plumes, with open access and delivery of data (Brenot et al., 2014; 2021),
48 but also the quantitative retrievals of volcanic ash as well as SO₂ concentration and altitude from satellite instruments, and
49 their validation.

50 Quantifying the SO₂ load emitted during explosive eruptions provides insight into volcanic processes, assists in volcanic hazard
51 mitigation and permits the climatic impact quantification of major eruptions (Carn et al., 2016). However, it is the accurate
52 retrieval of the SO₂ plume injection height that drives the majority of current scientific advancements in the field. Numerous
53 eruptions have already been used as demonstrational case studies using a variety of space-borne observations and modelling
54 techniques to infer the layer height such as eruptions by Mt Etna, Italy, (Boichu et al., 2015), Nabro, Erithrea, (Clarisse et al.,
55 2014), Jebel at Tair, Yemen (Eckhardt et al., 2008), Eyjafjallajökull and Grímsvötn, Iceland (Carboni et al., 2016), Calbuco,
56 Chile (Pardini et al., 2018), to name but a few.

57 Within the European Space Agency (ESA) Sentinel-5p+ Innovation SO₂ Layer Height project (S5P+I: SO2LH) activities have
58 led to the generation of a near-real-time SO₂ Layer Height product based on the Sentinel-5P/TROPOMI observations, hereafter
59 referred to as S5P SO₂ LH. In this work, we present the direct evaluation of the retrieved SO₂ layer heights for four recent

60 major eruptions against independent satellite information as well as its indirect verification via its assimilation into the
61 Copernicus Atmospheric Monitoring Service, CAMS, forecast system.

62 **2 S5P SO₂ Layer Height**

63 The retrieval of the SO₂ layer height based on Sentinel-5P/TROPOMI measurements is performed using the already established
64 “Full-Physics Inverse Learning Machine” algorithm (hereafter referred to as FP_ILM). It is based on Hedelt et al., 2019 and
65 is an improvement of the FP_ILM algorithm developed by Efremenko et al., 2017 for the retrieval of the SO₂ LH based on the
66 Global Ozone Monitoring Experiment, GOME-2, instrument data using a Principal Component Regression (PCR) technique.
67 In general, the FP_ILM algorithm creates a mapping between the spectral radiance and atmospheric parameters using machine
68 learning methods. The main advantage of the FP_ILM algorithm over classical direct fitting approaches is that the time-
69 consuming training phase involving complex Radiative Transfer (RT) modelling and Neural Network (NN) training is
70 performed offline; the final trained inversion operator itself is robust and computationally simple and therefore extremely fast
71 and can be applied in near-real-time (NRT) processing environments, as discussed in detail below. The FP_ILM algorithm
72 was originally developed for the retrieval of cloud properties (Loyola et al., 2006) and has also been used for the retrieval of
73 ozone profile shapes (Xu, et al., 2017) as well as the retrieval of surface properties accounting for bidirectional reflectance
74 distribution function (BRDF) effects (Loyola, et al., 2020.) Recently, Fedkin et al., 2020 have applied the FP_ILM algorithm
75 to retrieve the SO₂ LH based on Ozone Monitoring Instrument, OMI/Aura, observations.

76 The S5P SO₂ LH algorithm was further optimized in the framework of the ESA S5P+I: SO₂LH project. The S5P+I project has
77 been initiated to develop novel scientific and operational applications, products and retrieval methods that exploit the potential
78 of the Sentinel-5P mission’s capabilities beyond its primary objective and was kicked-off at the end of June/beginning of July
79 2019 and successfully finished at the end of 2021 and addresses seven themes related to atmospheric composition and ocean
80 colour. The SO₂LH theme is dedicated to the generation of an SO₂ layer height product for Sentinel-5p considering data
81 production timeliness requirements. More details about the project can be found on the ESA S5P+I website
82 (<https://eo4society.esa.int/projects/sentinel-5p+innovation/>, last access: 14.10.2021) as well as on the dedicated SO₂LH project
83 website (<https://atmos.eoc.dlr.de/so2-lh/>, last access: 14.10.2021), where all algorithm and product related documents are
84 publicly available.

85 **2.1 The optimised FP_ILM algorithm description**

86 The FP_ILM S5P SO₂ LH algorithm combines a Principal Component analysis (PCA) and a Neural Network (NN) approach
87 to retrieve the SO₂ LH based on Sentinel-5P/TROPOMI backscattered UV Earthshine measurements in the wavelength range
88 between 311 and 335 nm. The PCA is used to reduce the dimensionality of the high-resolution spectral measurements and to

89 extract the information related to the LH, whereas the NN is used to directly retrieve the LH based on the extracted principal
90 components (PCs) and other input parameters.

91 In a first step, the FP_ILM algorithm is trained using synthetic spectral UV data generated with the Linearized Discrete
92 Ordinate Radiative Transfer (LIDORT) model including inelastic rotational Raman scattering (RRS) implementation (Spurr
93 et al., 2008). About 500,000 reflectance spectra on a smart parameter grid (Loyola et al., 2016) in the wavelength range 311 -
94 335 nm have been generated, which are then convolved with the TROPOMI Instrument Spectral Response Function (ISRF).
95 This simulated dataset is split into two datasets: 90% is used for training the PCA and NN and the remaining 10% are set aside
96 and are used as an independent test dataset to determine the accuracy of the FP_ILM training. A PCA is then applied to the
97 training dataset to extract the first $N=10$ principle components to reduce the dimensionality of the spectral dataset. By
98 characterizing the set of simulated measurements with fewer parameters, a simpler, more stable and computationally efficient
99 inversion scheme can be realized.

100 In the second step, the PCs of each training sample along with the total ozone vertical column density (O_3 VCD), viewing
101 angles, surface pressure and albedo are used as input to train a feedforward artificial NN, with the corresponding SO_2 LH of
102 each training sample as the output layer. The NN consists of two hidden layers consisting of 40 nodes in the first and 10 nodes
103 in the second layer. A hyperbolic tangent layer activation function (tanh) is used and a regularization is applied to prevent the
104 NN from overfitting and to reduce the generalization error. Put together, the trained PCA operator and the trained NN form
105 the FP_ILM inversion operator, which is then applied to real spectral measurements in the operational phase.

106 In the operational phase, the trained PC operator is applied to TROPOMI spectral measurements which feature enhanced SO_2
107 levels, such as after a volcanic eruption, to extract the first 10 PCs and thus reduce the spectral dimension. With this information
108 (along with the other measured input parameters) the trained NN inverse function is then applied to retrieve the SO_2 LH. Note
109 that neither the SO_2 SCD nor the SO_2 VCD are input to the NN since they depend on the SO_2 LH both directly and indirectly
110 via the Air Mass Factor calculation and the temperature dependency of the absorption cross-section at the SO_2 layer altitude.

111 In the operational TROPOMI/S5P ground segment, Level 2 (L2) data is generated within 3 hours after sensing. Once this L2
112 data is available and a volcanic eruption occurs, the SO_2 LH algorithm is able to retrieve the corresponding layer height within
113 a few milliseconds per ground pixel. Even for a huge volcanic eruption with an SO_2 cloud spanning about 3% of the entire
114 orbit (i.e. about 50,000 pixels), the whole SO_2 LH retrieval is performed within 3 minutes. Note that the largest volcanic
115 eruptions detected by satellites so far (e.g., Raikoke, Kasatochi, Sarychev, Nabro) lead to typically 1-3% of ground pixels to
116 be processed for a limited number of orbits. The FP_ILM algorithm is several orders of magnitude faster than any of the direct
117 fitting approaches for UV layer height retrievals developed so far.

118 Closed-loop retrievals with the independent test dataset show that the SO_2 LH can be retrieved with an accuracy of less than 2
119 km for SO_2 VCD > 20 Dobson Units, D.U., (see Hedelt et al., 2019; SO_2 LH Algorithm Theoretical Baseline Document, ATBD,
120 Hedelt et al., 2021 and SO_2 LH Validation Report, VR, Koukouli et al., 2021). Note here that in the presence of volcanic ash,
121 which can be initially collocated with the SO_2 cloud in the young volcanic plume, the retrieved SO_2 LH can be underestimated

by several kilometres since the FP_ILM inversion operators were trained without taking ash absorption into account (see an extensive discussion in S5P SO₂ LH ATBD, Hedelt et al. 2021). From the analysis presented in the S5P SO₂ LH VR (Koukouli et al., 2021) it was deduced that the optimal accuracy was achieved when filtering the reported LH values using a QA value (indicating the quality of the retrieval) greater than 0.5, a LH flag (indicating warnings and errors during the retrieval) less than 16 and an associated SO₂ load greater than 20 D.U. For the comparison against the independent datasets, the SO₂ LH were then gridded onto a 0.1x0.1° spatial plane at 6h intervals per eruptive day.

3 Comparative datasets

Two different IASI/Metop SO₂ layer heights (LHs) are used for the evaluation of the S5P SO₂ LHs: the EUMETSAT ACSAF Brescia v201510 product (Clarisse et al., 2012; 2014; Astoreca et al., 2018), here after IASI ULB/LATMOS, as well as the University of Oxford product (Carboni et al., 2012; 2016), hereafter IASI AOPP. The two IASI approaches vary to such an extent, as is discussed below, that we can assume that they provide two semi-independent datasets available for the validation of the S5P SO₂ LHs. In addition, the CALIOP/CALIPSO space-born lidar observations of the ash plume (Winker et al., 2012; Prata et al., 2017) will be compared to the S5P SO₂ LHs for the case of the Raikoke stratospheric eruption. Furthermore, the S5P SO₂ LH product was assimilated into a Copernicus Atmosphere Monitoring Service, CAMS, experiment (Inness et al., 2022), and the assimilated fields were compared to the independent IASI ULB/LATMOS observations, indirectly validating the S5P SO₂ LH v4.0 product.

3.1 IASI ULB/LATMOS SO₂ Layer Height dataset

The IASI/MetOp SO₂ ACSAF column data are fully described in Clarisse et al., 2012, where a algorithm for the sounding of volcanic SO₂ plume above ~5 km altitude was presented and applied to IASI. The algorithm is able to view a wide variety of total column ranges (from 0.5 to 5000 D.U.), exhibits a low theoretical uncertainty (3–5 %) and near real time applicability and was thence demonstrated on the eruptions of Sarychev in Russia, Kasatochi in Alaska, Grimsvötn in Iceland, Puyehue-Cordon Caulle in Chile and Nabro in Eritrea. Furthermore, an expansion of the algorithm to also provide SO₂ LHs for the Nabro eruption using forward trajectories and CALIOP coincident measurements is described in Clarisse et al., 2014. The IASI ULB/LATMOS dataset includes five SO₂ column data at assumed layer heights of 7, 10, 13, 16 and 25 km, as well as a retrieved best estimate for the SO₂ LH. It is important to note that the SO₂ LHs provided by this algorithm are quantized every 0.5 km, which renders simple scatter-type comparisons not as straightforward. This dataset is publicly available from <https://iasi.aeris-data.fr/>. The observations by all Metop IASI instruments were treated as one, gridded onto a 0.1x0.1 grid at 6h intervals or each day. The choice of the temporal field was applied since the S5P and Metop orbits differ on average by 3-4h and this temporal range

was found to be the optimal trade-off between resulting in a successful collocative dataset while also ensuring the comparisons view the same parts of the SO₂ plumes. Recall also that IASI, an infrared sounder, also performs observations 12h later, during night-time. For high enough latitudes, the time zones collapse onto another, so in the case of high latitude volcanoes, such as Raikoke, a collocation closer in time can be achieved. For this dataset, the reported SO₂ LHs were restricted to altitudes less than 25 km where a successful SO₂ column retrieval was performed.

3.2 IASI AOPP SO₂ Layer Height dataset

The University of Oxford employs an optimal estimation scheme (Carboni et al. 2012; 2016) to estimate the SO₂ column amount, the height of the SO₂ profile and the surface radiating temperature from IASI/MetOp-A, /MetOp-B & /MetOp-C measurements. The Oxford retrieval has two steps. Firstly, a linear retrieval developed by Walker et al. (2011; 2012) is applied. In the retrieval scheme a detection is considered ‘positive’ if the output of the linear retrieval is greater than a defined positive threshold (0.49 effective DU, following Walker et al. 2012). The detection limits are variable-dependent on the height of the plume and the atmospheric conditions. For a standard atmosphere (with no thermal contrast) the detection limits are estimated to be: 17 D.U. for a SO₂ plume between 0-2 km, 3 D.U. between 2-4 km, and 1.3 D.U. between 4-6 km (Walker et al., 2011). The detection scheme can miss part of an SO₂ plume under certain circumstances, such as low-altitude plumes, conditions of negative thermal contrast (i.e. where the surface is colder than the atmosphere), and where clouds are present above the SO₂ plume, masking the signal from the underlying atmosphere. The IASI SO₂ retrieval is not affected by underlying clouds. Secondly, an iterative retrieval is performed for the pixels that provide positive detection results. The scheme iteratively fits the forward model (simulations) with the measurements, through the error covariance matrix, to seek a minimum of a cost function. The forward model is based on RTTOV (Radiative Transfer for TOVS) which is a very fast radiative transfer model for passive visible, infrared and microwave downward-viewing satellite radiometers, spectrometers and interferometers (Saunders et al., 1999). The error covariance matrix used is the ‘global error covariance matrix’ described by Carboni et al., 2012, defined to represent the effects of atmospheric variability not represented in the forward model (FM), as well as instrument noise. A comprehensive error budget for every pixel is included in the retrieval.

A quality control was applied to the IASI AOPP dataset to include valid data points where the minimization routine converged within 10 iterations, the retrieved SO₂ amount was positive, the retrieved plume pressure was between 0 and 1100 mb and the cost function was less than 10. Additional filters were applied in this work to include only pixels with SO₂ LH \leq 25 km, SO₂ LH error \leq SO₂ layer height and the retrieved altitude \neq a priori altitude at 400 mbars. The latter would indicate that the retrieval reverted back to the a priori for lack of signal in the measurement, hence would not provide any novel information to the retrieval. After the additional filters were applied, the IASI/AOPP dataset was also gridded onto a 0.1x0.1 grid at 6h intervals per eruptive day.

182 **3.3 CALIOP/CALIPSO Volcanic Layer Height dataset**

183 CALIPSO (*Cloud-Aerosol and Lidar Infrared Pathfinder Observations*), is a joint NASA/CNES (Centre National d' Études
184 Spatiales) satellite and part of the A-Train constellation of satellites. It is designed to study aerosols and clouds and aims to
185 provide profiling information at a global scale for improving our knowledge and understanding of the role of the aerosols in
186 the atmospheric processes. The main instrument, CALIOP (*Cloud-Aerosol Lidar with Orthogonal Polarization*), is a dual-
187 wavelength (532 and 1064 nm) elastic backscatter lidar with the capability of polarization-sensitive observations at 532 nm
188 (Winker et al., 2010). The high-resolution profiling ability coupled with accurate depolarization measurements make
189 CALIPSO an indispensable tool to monitor specific aerosol species and clouds (Liu et al., 2008). CALIPSO is the first
190 polarization lidar to provide global atmospheric measurements and is able to identify volcanic eruption plumes related to the
191 SO₂ Layer Height identification and retrieval (e.g. Fedkin et al., 2021; Hedelt et al., 2019; Koukouli et al., 2014; Tournigand
192 et al., 2020). The CALIPSO observations close to the volcanic source can be employed in SO₂ LH validation studies, since
193 ash (and/or aerosols) are initially collocated with the SO₂ cloud, before the gas and ash plumes separate. Note that the footprint
194 of CALIOP measurements is only 100 m, hence the global coverage is very low and detection of a volcanic ash plume is rare.
195 The CALIOP optical properties retrieval scheme is based on the successful cooperation of three major algorithm steps whose
196 main mission objective is to produce the CALIPSO Level 2 (L2) data (Vaughan et al., 2009, Omar et al., 2009). Finally,
197 CALIPSO data consist of three basic types of information: (a) layer products, (b) profile products and (c) the vertical feature
198 mask (VFM). Layer products provide layer-integrated or layer-averaged properties of detected aerosol and cloud layers. Profile
199 products provide retrieved extinction and backscatter profiles within these layers. Because information on the spatial locations
200 of cloud and aerosol layers is of fundamental importance, the VFM was developed to provide information on cloud and aerosol
201 locations and types. Layer properties include layer top and base altitude, as well as physical properties of the feature such as
202 the Integrated Volume Depolarization Ratio, some of which are described below. Layer top and base altitudes are reported in
203 units of kilometres above mean sea level. Between -0.5 km and ~8.2 km, the vertical resolution of the lidar is 30-meters. From
204 ~8.2 km to ~20.2 km, the vertical resolution of the lidar is 60-meters. Above ~20.2 km, the vertical resolution is 180-meters.
205 The on-board averaging scheme provides the highest resolution in the lower troposphere where the spatial variability of clouds
206 and aerosols is the greatest and coarser resolutions higher in the atmosphere The CALIPSO data products used in this validation
207 study are summarized in Table 1.

208
209 **Table 1. CALIOP/CALIPSO parameters used in this study.**

Parameter	Version	Level	Resolution Due to Averaging	
			Horizontal	Vertical (<8 km)
Total_Attenuated_Backscatter_532	v.4.10	1	1/3 km	30 m
Extinction_Coefficient_532	v.3.41, v.4.20	2	5 km	60 m

Aerosol_Layer_Top/Base_Altitude	v.3.41, v.4.20	2	5 km	30 m
Feature_Classification_Flags	v.3.41, v.4.20	2	5 km	60 m

The CALIPSO version 4 (V4) product determines the locations of layers within the atmosphere, discriminates aerosols from clouds and categorizes aerosol layers as one of eleven subtypes, seven in the troposphere and four in the stratosphere (Omar et al., 2009; Kim et al., 2018) providing also the optical depth of each detected aerosol layer (Winker et al., 2012). The most fundamental update in V4 is that aerosol layers are now classified as either tropospheric aerosol or of certain stratospheric aerosol feature types. The tropospheric aerosol types include the following sub-types: clean marine, dust, polluted, continental/smoke, clean continental, polluted dust, elevated smoke and dusty marine. Stratospheric aerosol subtypes have been introduced for ash, sulfate/other, smoke and polar stratospheric aerosol. Note that below the tropopause, ash and sulphate plumes are given by the tropospheric aerosol subtypes: volcanic ash is often classified as dust or polluted dust and volcanic sulphate is often classified as elevated smoke. As a result, contiguous aerosol features crossing the tropopause will have aerosol subtypes which switch from tropospheric to stratospheric subtypes, depending on the relationship between the attenuated backscatter centroid altitude of the layer identified by the feature finder and the tropopause altitude. Refer to the Data Quality Summary Document for further details (Vaughan et al., 2020).

3.3.1 CALIOP weighted extinction height

An important indicator for vertical profiles is the weighted extinction height, a parameter that gives in a single number an indication of the altitude of the detected aerosol plume distribution. This parameter is considered ideal for comparisons with aerosol layer height from passive satellite sensors (e.g. GOME-2, IASI, TROPOMI) and the future Sentinel missions, since these retrievals are very sensitive to the location of the aerosol mass maximum within the detected layers. For the validation of the TROPOMI SO₂ LH, we used CALIOP level 2 version 4.10 aerosol extinction profiles at 5 km spatial resolution, retrieved from CALIOP observations of attenuated backscatter at 532 nm (Winker et al., 2010). Quality flags are also included in the level-2 CALIOP products and are used to avoid cloud contamination of aerosol retrievals, which means that cloud features are identified and removed, as described in Winker et al. (2013) and Campbell et al. (2012).

To facilitate quantitative comparison of aerosol altitude, we used a mean extinction height calculated from the CALIOP extinction profile, following Koffi et al. (2012):

$$ALH_{ext} = \frac{\sum_{i=1}^n \beta_{ext,i} Z_i}{\sum_{i=1}^n \beta_{ext,i}} \quad \text{Equation 1}$$

where Z_i is the height from sea level in the i^{th} lidar vertical level i (km), and $\beta_{ext,i}$ is the aerosol extinction coefficient (km^{-1}) at the same level. In the CALIOP level 2 products, aerosol extinction is only retrieved for the layers in which aerosols are detected, depending on the instrument's signal-to-noise ratio (SNR). In the case when aerosols are present over clouds, ALH_{ext} will be situated in the centre of the aerosol layer, with any undetected aerosol layers below the cloud layer not included in the calculations due to attenuation of the signal beyond the cloud layer. According to this validation method, the CALIOP 532nm

channel observations are chosen for analysis as the conclusions from the analysis of the results do not change when the 1064 nm channel observations are used instead (Nanda et al., 2020).

4 Results

4.1 Comparisons with the IASI/Metop SO₂ Layer Heights

4.1.1 Raikoke, 2019

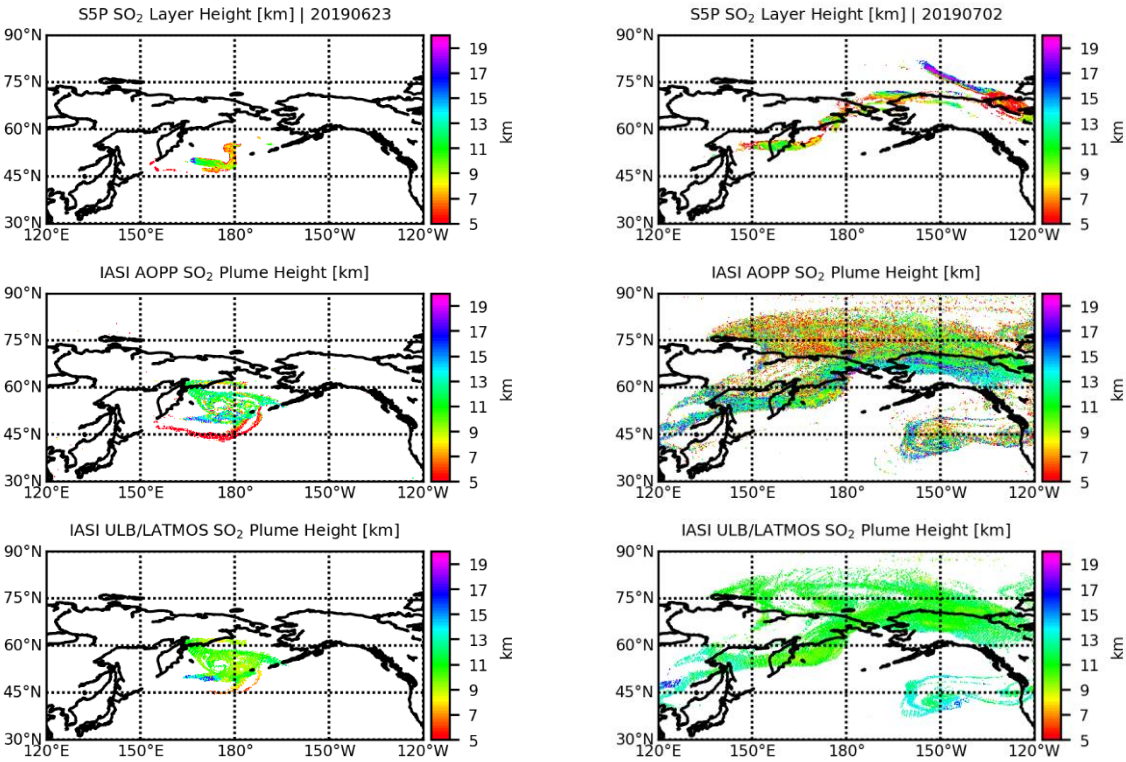


Figure 1. SO₂ Plume Height for two example days of the Raikoke 2019 eruptive period, the 23rd of June on the left and the 2nd of July on the right. The S5P+I: SO₂ LH at the top, IASI AOPP LH in the middle and IASI ULB/LATMOS LH on the bottom panels, including both ascending and descending orbits.

On June 22nd, 2019, a vast plume of ash and volcanic gases with more than 1000 D.U. of SO₂ was emitted during the eruption of the Raikoke volcano, Kuril Islands (McKee et al., 2021). This eruption could be detected even two months after the end of eruptive event, which rendered it an important case study for testing different satellite observations retrieval methods; the

original FP_ILM methodology applied to TROPOMI observations (Hedelt et al., 2019), a probabilistic enhancement method using the Cross-track Infrared Sounder (CrIS) on the Joint Polar Satellite System (JPSS) series of satellites (Hyman and Pavolonis, 2020), a synergistic analysis of different satellite observations and dispersion modelling (Kloss et al., 2021) and the recent application of the FP_ILM algorithm to OMI/Aura observations (Fedkin et al., 2021.) This eruption was also used in numerical atmospheric modelling in simulating the dispersion of the Raikoke SO₂ cloud in the UK Met Office Numerical Atmospheric-dispersion Modelling Environment (de Leeuw et al., 2021) and the Copernicus Atmosphere Monitoring Service (Inness et al., 2022).

In Figure 1, two example days of the 2019 Raikoke eruption, the 23rd of June (left) and the 2nd of July (right) are shown for the S5P SO₂ LH (upper), the IASI AOPP LH (middle) and the IASI ULB/LATMOS LH (bottom) observations. These demonstrational figures do not represent collocative datasets, but rather show the spatial extent of the plumes reported by each dataset, after filtering and gridding are performed. Due to the restriction in SO₂ load necessary (> 20 D.U.) in the S5P SO₂ LH algorithm, the thinner parts of the plumes are not captured by the S5P observations, however its near-real-time capabilities renders it an excellent tool for early detection in view of aviation safety. The equivalent maps for the SO₂ load are presented in Figure S1, where it is shown that the extensive plumes reported by both IASI products are associated with loads of less than ~ 20 D.U. A point to stress here is the undeniable fact that the S5P LH is retrieved in the UV wavelength range, which is sensitive to other atmospheric levels than the IR based LH retrieval based on IASI data, hence different parts of the volcanic cloud are sensed. Although the IASI LH gives a first estimate of the height of the volcanic cloud, this information cannot be used in S5P SO₂ retrievals due to the difference in overpass time and pixel resolution. As the main limitation of the S5P LH product is that it can only be applied to modest to high volcanic eruptions, with SO₂ VCD > 15 -20 DU, weak volcanic eruptions, or the weaker parts of cannot SO₂ plumes cannot be retrieved. This point explains the different plume structure shown in Figure S1.

The vertical distribution of the Raikoke SO₂ plume can be examined in the integrated SO₂ mass profiles presented in Figure 2. The reported SO₂ load was integrated every 1 km, between 0 and 20 km, on the collocated gridded datasets. In these two eruptive days, we note how the SO₂ mass dispersed is placed with respect to the retrieved layer height among the three datasets. Overall, the location of the peak SO₂ mass is within 2 km between S5P and IASI, however for the case of the IASI AOPP the amount of ejected SO₂ mass is systematically lower in magnitude, even though it is well placed in height. This is most likely linked to the quality control applied to the IASI AOPP SO₂ results which excludes a number of pixels within the core part of the plume, due to the poor fit between the measured and modelled spectra.

280

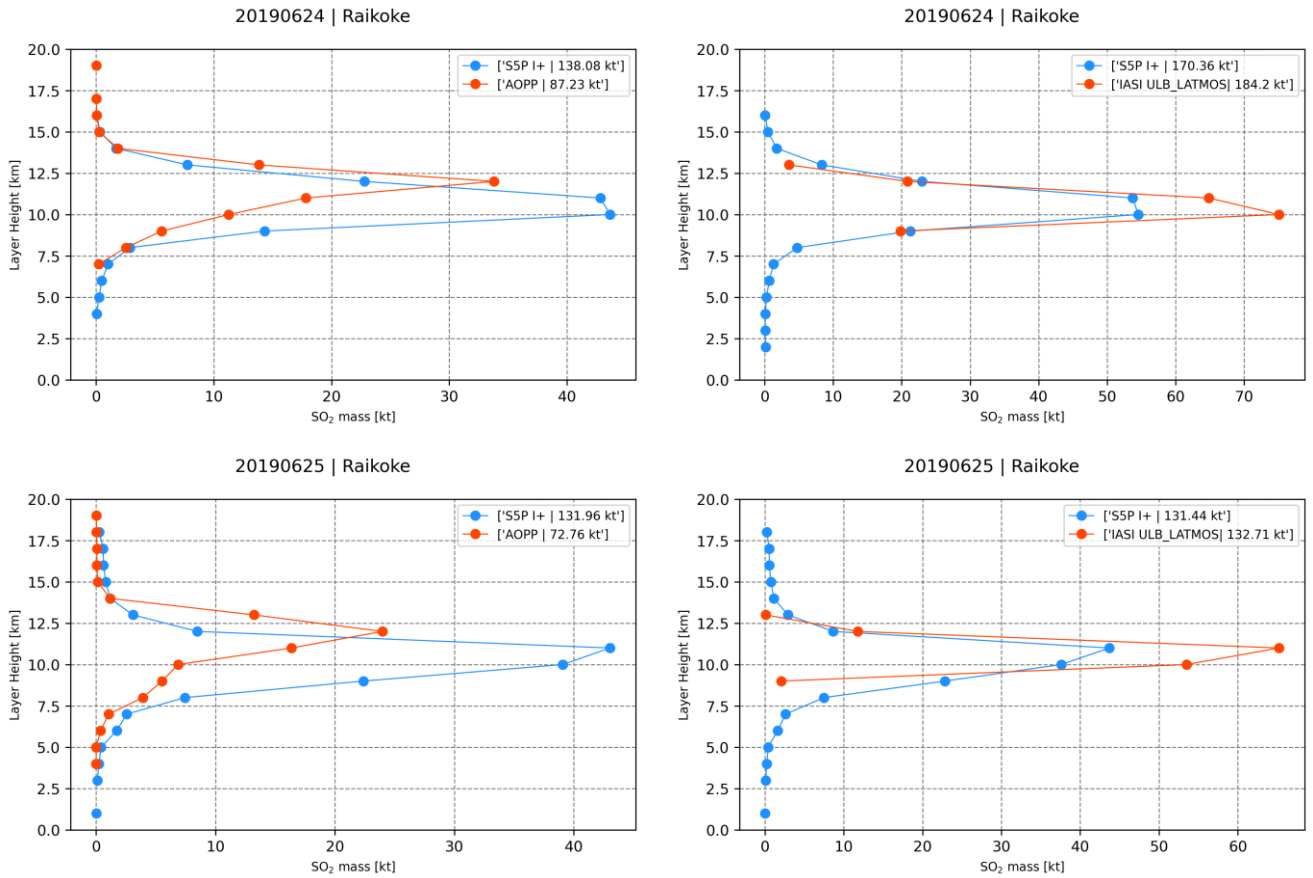


Figure 2. SO₂ integrated mass (kt) against plume altitude (km) for two example days of the Raikoke 2019 eruptive period, the 24th (upper row) and the 25th of June (lower row) for the S5PSO₂ LH product in blue and the IASI AOPP in red (left column) and IASI ULB/LATMOS in red (right column). In each set, the respective collocations are shown.

Figure 3 shows the comparisons for the entire Raikoke eruptive period between the S5P SO₂ LH and the IASI/AOPP LH (left) and the IASI ULB/LATMOS LH (right) in histogram mode. For both comparisons, the mean S5P SO₂ LH is reported at 10.75 ± 3.50 km for the IASI/AOPP and at $\sim 10.20 \pm 2.80$ km for the IASI ULB/LATMOS collocations. IASI/AOPP places the plume at $\sim 11.40 \pm 2.50$ km and IASI ULB/LATMOS at $\sim 10.00 \pm 1.0$ km, resulting in an excellent mean difference between sensors of $\sim \pm 0.5 \pm 3$ km on average.

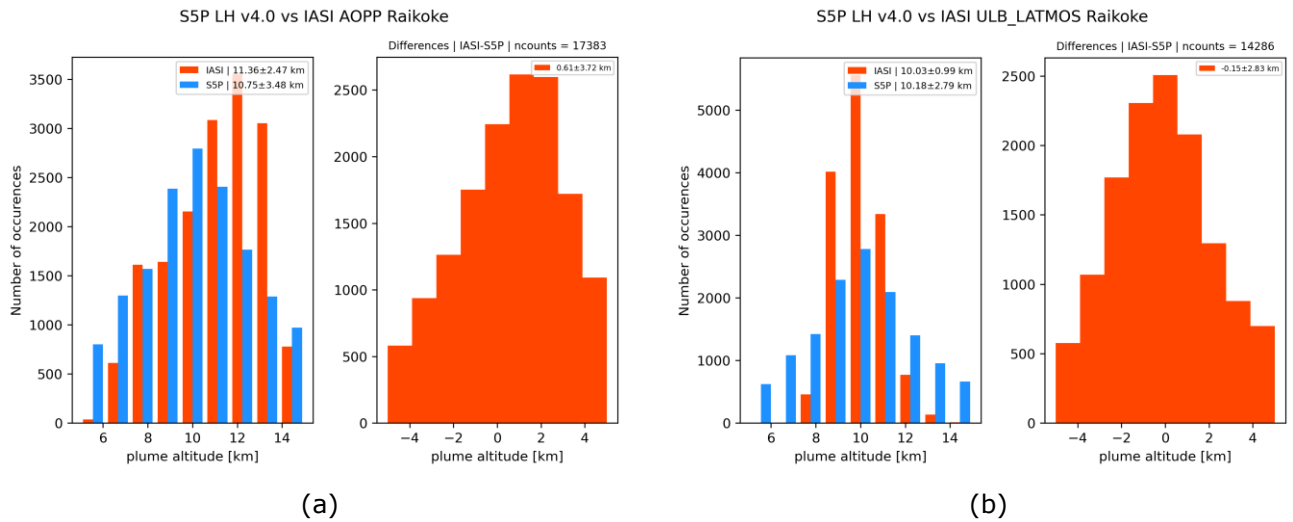


Figure 3. Comparisons between spatiotemporally collocated plume heights for the Raikoke, 2019, eruptive days. (a), left panel, histogram distribution for the S5P LHs (blue) and the IASI/AOPP LHs (orange) and right panel, their absolute differences. (b) as per (a) for the comparisons to the IASI ULB/LATMOS dataset.

4.1.2 Taal, 2020 and La Soufrière, 2021 eruptions

The Taal volcano in Batangas, Philippines erupted on the afternoon of January 12th, 2020, 43 years after its previous eruption in 1977. Stronger explosions began around 3 pm and spewed an ash column exceeding a kilometre in thickness. By 7:30 pm, volcanic activities intensified as continuous eruptions generated a tall, 10 to 15 kilometres, steam-laden tephra column (Jing et al., 2020). Perttu et al., 2020, analysed infrasound observations to the East of the volcano and estimated a plume height and duration for further ash dispersion modelling, reporting the plume at a mean height of 15 km. The High Spectral Resolution Lidar of the Manila Observatory (<http://www.observatory.ph/2020/01/17/taal-volcano-2020-eruption-impact-on-air-quality-part-i/>, last access 13.10.2021) reported a massive ash cloud ingested and transported above the 12 km altitude in the first post eruption hours, a finding further corroborated by the volcanic ash detected by the Advanced Meteorological Imager on board the GEOKOMPSAT-2A platform (Ahn et al., 2021) whose analysis also placed the ash cloud at 12 km. The presence of ash hinders the detection of the SO₂ cloud by both UV-visible and infrared sensors and partially explains the larger spread in reported SO₂ layer heights by TROPOMI and IASI shown in Figure S2. A large disagreement on the altitude of the SO₂ plume is found between datasets in this case, with differences between -3 and -5 km between the observations, also attributable to the ~3h difference in sensing time and its importance when studying the first few hours after a volcanic eruption (see maps in Figure S3).

On the morning of April 9th 2021, the La Soufrière volcano on the Caribbean island of Saint Vincent began erupting, spewing ash at least 7.5 km in the air, for the first time since 1979. The volcano continued to erupt over the next several days, with multiple violent explosions. Ash blanketed Saint Vincent and winds carried ash to Barbados, about 120 miles east. The

Smithsonian Institute Global Volcanism Program, <https://volcano.si.edu/volcano.cfm?vn=360150>, last access: 13.10.2021, reported a period of explosive activity and strong pulses of ash emissions at 03:30 on the 10th April, whose resulting ash plumes rose to ~10-16 km altitude throughout the day. On the 12th of April, at 04:15, another large explosion produced an ash plume that rose to ~13 km altitude. The spread of the SO₂ plume sensed by TROPOMI and both IASI algorithms is shown in Figure S4, where the SO₂ plume reached very high altitudes, above 15 km, when close in location to the volcano and decreasing in height as it progressed to the East over the sea. For both comparisons in Figure S5, the agreement of the collocative datasets is within 1 km, all instruments placing the SO₂ plume at an average height of 14-15 km.

4.1.3 Summary of the comparisons with the IASI/Metop observations

The overall statistics for the comparisons of the SO₂ plume altitude for four eruptions between 2019 and 2021 for S5P and the IASI AOPP comparisons are shown in Table 2 while those of the IASI ULB/LATMOS are given in Table 3. The collocations refer each time to those of each of the two sets. Note that for the Nisinoshima, Japan, eruptive period in July & August 2020, collocations are only available for the IASI ULB/LATMOS datasets. Overall, per eruptive period, the mean plume altitudes are similarly placed by both UV-visible and infrared instruments, with a mean difference of ~0.20±3.30 km for the Raikoke, Nishinoshima and La Soufrière and ~ -3.60±2.90 km for the Taal eruption.

Table 2. Overall statistics for the comparison between S5P and IASI AOPP for the eruptive periods.

	Mean S5P LH	Mean IASI AOPP LH	Mean Difference	Collocations no.
Raikoke, 2019	10.75±3.48 km	11.36±2.47 km	0.61±3.72 km	17383
Taal, 2020	10.14±3.5 km	5.64±1.5 km	-4.49±2.82 km	47
La Soufrière, 2021	13.82±2.49 km	13.47±3.41 km	-0.35±3.55 km	25

Table 3. Overall statistics for the comparison between S5P and IASI ULB/LATMOS for the eruptive periods.

	Mean S5P LH	Mean IASI ULB/LATMOS LH	Mean Difference	Collocations no.
Raikoke, 2019	10.18±2.79 km	10.03±0.99 km	-0.15±2.83 km	14286
Taal, 2020	12.13±3.95 km	9.51±1.78 km	-2.62±3.0 km	17
Nishinoshima, 2020	7.73±1.97 km	8.0±1.04 km	0.27±2.79 km	11
La Soufrière, 2021	14.94±3.87 km	15.7±1.16 km	0.76±3.69 km	168

The comparisons between S5P and IASI AOPP SO₂ LHs is shown, in Figure 4, left, and IASI ULB/LATMOS on the right, for all eruptive days where the mean plume height reported for each of the 27 days of collocations is shown as a scatter plot. For the IASI AOPP SO₂ LHs, left, the comparison is very promising, with a slope close to 0.91±0.21, y-intercept of 1.20±2.54 km and correlation coefficient of 0.66 for the 27 collocations days for the Raikoke, Taal and La Soufriere eruptions. The outlier

point, where S5P reports a high layer height at ~10 km while IASI AOPP reports low at ~5 km, belongs to the Taal comparison, discussed previously. For ULB/LATMOS comparison, the mean SO₂ LHs, as expected, follow a straight line, with slope of ~0.98±0.19 and y-intercept of ~0.77±2.06 km, and a correlation coefficient of 0.73. Nearly 20 days belong to the Raikoke eruptive period, and the rest to the Taal, Nishinoshima (only for ULB/LATMOS) and La Soufriere eruptions.

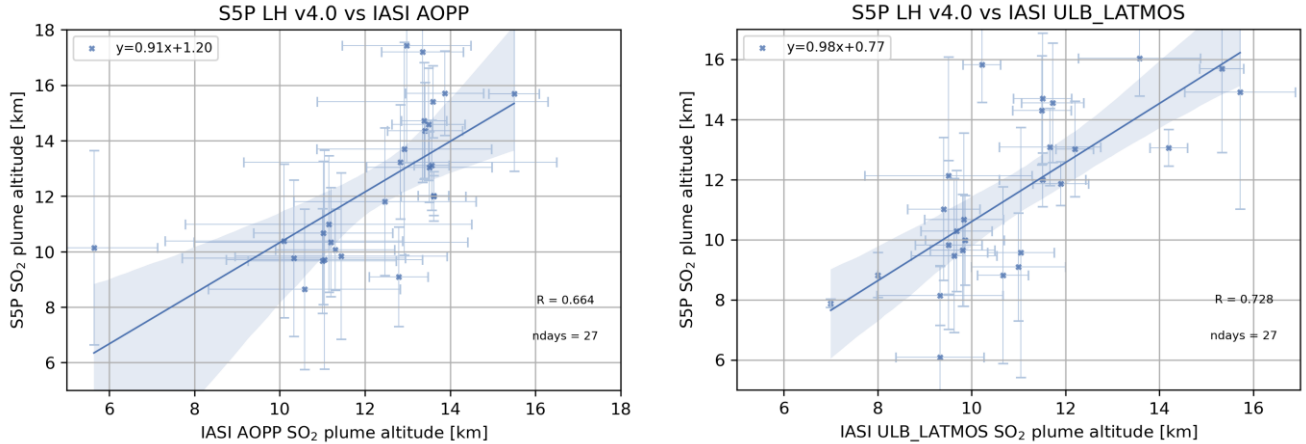


Figure 4. Scatter plot of the mean daily average reported SO₂ LHs by TROPOMI/S5P and IASI/AOPP (left) and IASI ULB/LATMOS (right) for all available collocated eruptive days. The error bars represent the standard deviation of the mean while the shaded areas represent the 95% confidence interval of the fit.

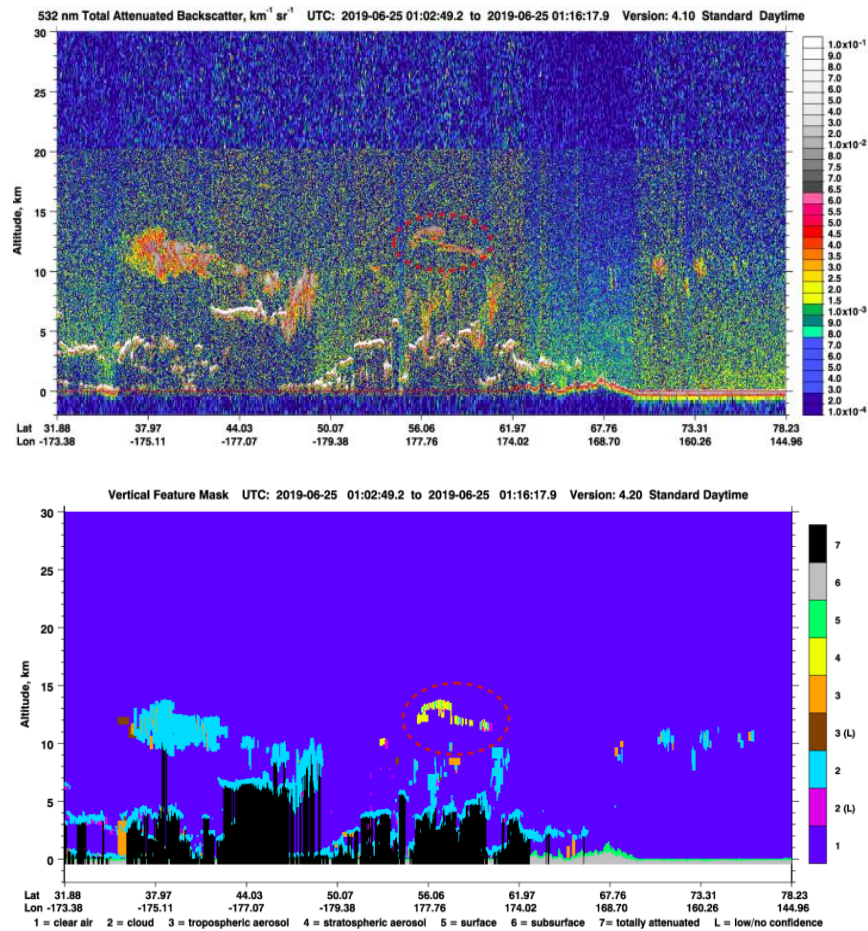
4.2 Comparisons with CALIOP/CALIPSO Volcanic Ash Layer Height

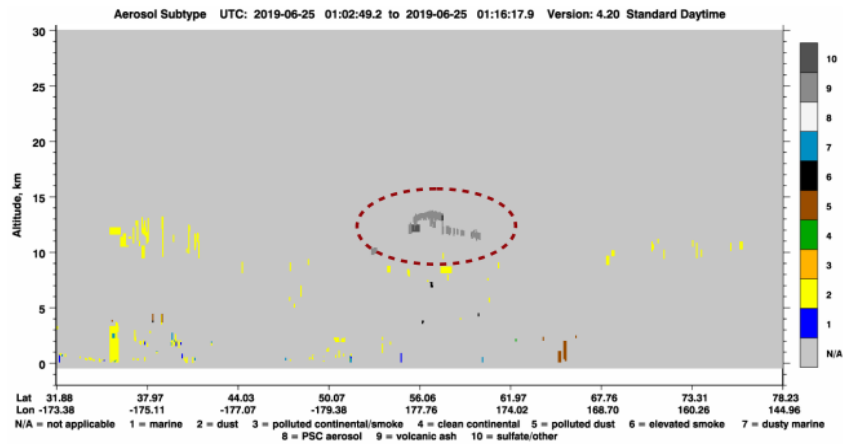
4.2.1 Raikoke, 2019

Within this study, the availability of overpasses of CALIPSO/CALIOP after the eruption of the Raikoke volcano on the 22nd of June was examined. Volcanic ash and sulphate aerosols are identified in CALIOP profiles based on collocated TROPOMI pixel values. The closest distances between the CALIOP footprint of the CALIPSO overpass and the locations of the TROPOMI centre pixels are selected respectively, to create collocated datasets, usually with the two orbits being within 1h to one another. To illustrate the reliability of the TROPOMI SO₂ LH product, we discuss in detail a selected case of collocated and concurrent TROPOMI – CALIPSO observations close to the detected SO₂ plume from the Raikoke eruption, on the 25th of June 2019.

We use the 532 nm Total Attenuated Backscatter (TAB) data version 4.10 from one CALIPSO orbit in order to detect the aerosols and clouds and their heights. The TAB signal strength (Figure 5, top) is color-coded in a manner that the blue background represents molecular and weak aerosol scattering while aerosols typically appear in the shades of red, orange and yellow. The grey scales represent the stronger cloud signals, while the weaker cloud signals, being similar in strength to the

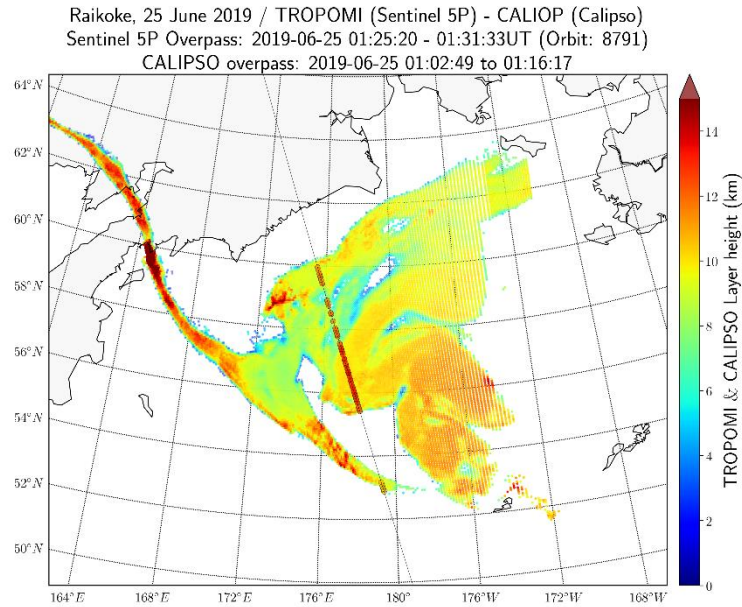
356 strong aerosol signals, also appear in the shades of red, orange and yellow. The TAB is sensitive to both water and ice droplets,
 357 as well as numerous types of atmospheric particles. The equivalent VFM image (Figure 5, middle) shows the aerosol type,
 358 which is retrieved according to the aerosol classification algorithm for all the detected aerosol layers. The VFM describes the
 359 vertical and horizontal distribution of both aerosols and clouds. After detection of the aerosol features, they are then classified
 360 into types and subtypes. As shown in Figure 5 (bottom), the plume scene is well captured and according to the V4 algorithm,
 361 is classified as volcanic ash/ sulphate (Kim et al., 2018). The volcanic plume of the 25th of June 2019 is marked with a dashed
 362 red circle.
 363



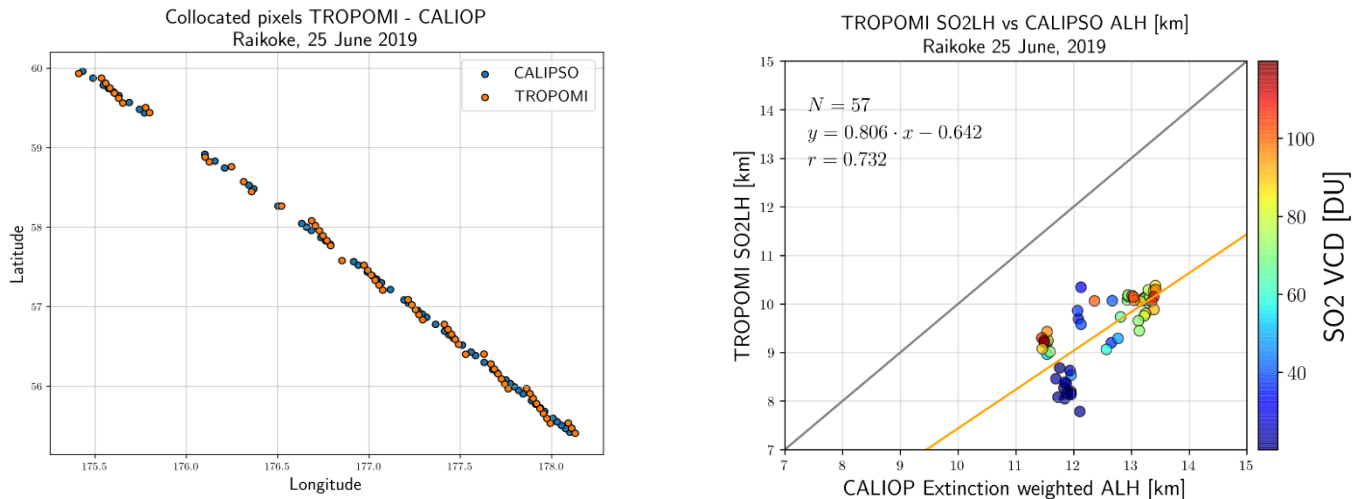


364 **Figure 5.** CALIOP lidar measurements for the Raikoke eruption along the track indicated in Figure 6 on the 25th of June
 365 2019. (Top) Total attenuated backscatter profile (in $\text{sr}^{-1} \text{km}^{-1}$), (middle) Vertical Feature Mask image showing the location of
 366 all layers detected and (bottom) aerosol subtype. The red dashed circles denote the volcanic feature detected from CALIOP.
 367 Images courtesy of NASA: <https://www-calipso.larc.nasa.gov/products/>

368 Figure 6 shows the TROPOMI SO_2 layer height pixels retrieved by the FP_ILM algorithm for SO_2 VCDs greater than or equal
 369 to 20 DU, $\text{QA} > 50$ and $\text{LHflag} < 16$, overlaid with the calculated CALIPSO weighted extinction ALH pixel values (coloured
 370 circles) which are color-coded according to the range of height values (in km). The CALIOP overpass time of this area is
 371 between 01:00 and 01:15 UTC, and the TROPOMI overpass time is between 01:25 and 01:30 UTC, a time difference of mere
 372 minutes. The TROPOMI plume shows several layers with SO_2 layer heights ranging from 5-6 km up to 14 km for this day. In
 373 the area of the plume observed by both TROPOMI and CALIOP ($54 - 58^\circ\text{N}$ & $176 - 178^\circ\text{E}$), the CALIOP vertical feature
 374 mask and aerosol subtype mask identify some volcanic ash at approximately 13 km altitude, and meteorological clouds mixed
 375 with tropospheric aerosols (dust, polluted dust and elevated smoke) at lower altitudes. The clouds below the ash plume are
 376 shown in blue in Figure 5, middle panel.



377 **Figure 6.** TROPOMI SO₂ layer height for the Raikoke volcanic eruption, measured on the 25th of June 2019. Only pixels with
378 SO₂ VCDs greater than or equal to 20 D.U. are shown. The black line indicates the CALIPSO ground track and the coloured
379 circles along the line indicate weighted extinction height product values (in km), for the results shown in Figure 5.



380 **Figure 7.** Left. The latitude/longitudes of the collocated pixels. Right. Comparison between TROPOMI SO₂ LH and CALIPSO
381 weighted extinction height for the 25th of June 2019, colour-coded depending on the TROPOMI SO₂ column amount. The
382 orange line is the regression line of the TROPOMI-CALIPSO observations; the grey line is the 1:1 line.

383
384
385
386
387
388
389
390
391
392
393
394
395
396
397
398
399
400

401
402
403

The spatiotemporal collocation between TROPOMI and CALIOP on that day is near perfect (Figure 7, left) and the spatial agreement between SO₂ LH and CALIOP weighted extinction altitude is satisfactory, considering the differences between the ash and SO₂ plumes, confirming the presence of volcanic plumes. Both instruments yield high altitude values, however TROPOMI retrieves higher altitudes especially for the western part of the plume. A comparison scatterplot of collocated ash-flagged pixels is shown in Figure 7, right. The pixel-by-pixel scatter of the 57 common points shows a high correlation of 0.73, even though the SO₂ plume is placed approximately 2 km lower than the ash plume.

Overall, seven TROPOMI (at 22/6 02:20; 23/6 00:20; 24/6 00:00; 25/6 01:30; 28/6 02:00; 29/6 02:00 and 30/6 01:30) and CALIPSO collocated overpasses (at 22/6 02:30; 23/6 01:30; 24/6 00:30; 25/6 01:00; 28/6 03:00; 29/6 03:35 and 30/6 02:40) were identified. A statistical analysis has been performed using all resulting 241 collocated pixels for the 22nd, 23rd, 24th, 25th, 28th, 29th and 30th of June 2019. Figure 8 shows the distribution of TROPOMI SO₂ LH and CALIOP calculated weighted height differences for all days, as a scatter plot on the left and on a histogram representation on the right. The coloured dots in the scatter plot denote each individual eruptive day. The overall agreement is adequate and as expected, with mean and median residual values around ~-2.4 km and ~-3.0 km respectively, and standard deviation of ~1.7 km. The CALIOP ALH_{ext} is higher than TROPOMI SO₂ LH in the majority of the cases. This could partially be due to CALIOP underestimating the aerosol layer thickness due to strong attenuation of the lidar signal at the top of the detected aerosol layer (Rajapakshe et al., 2017), whereas the TROPOMI SO₂ LH product does not suffer from such attenuation.

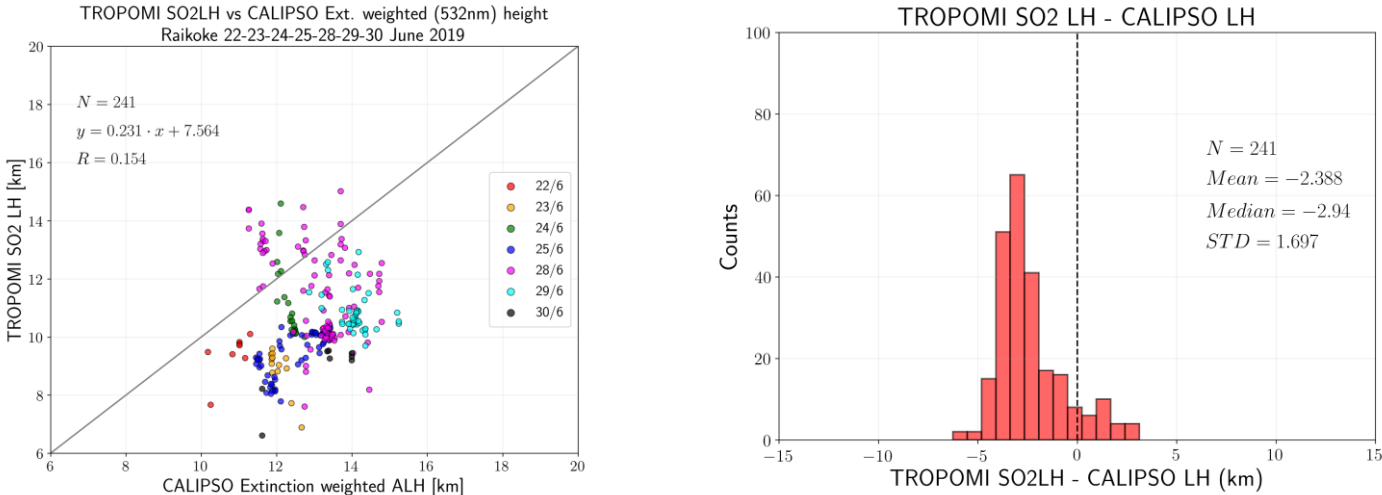
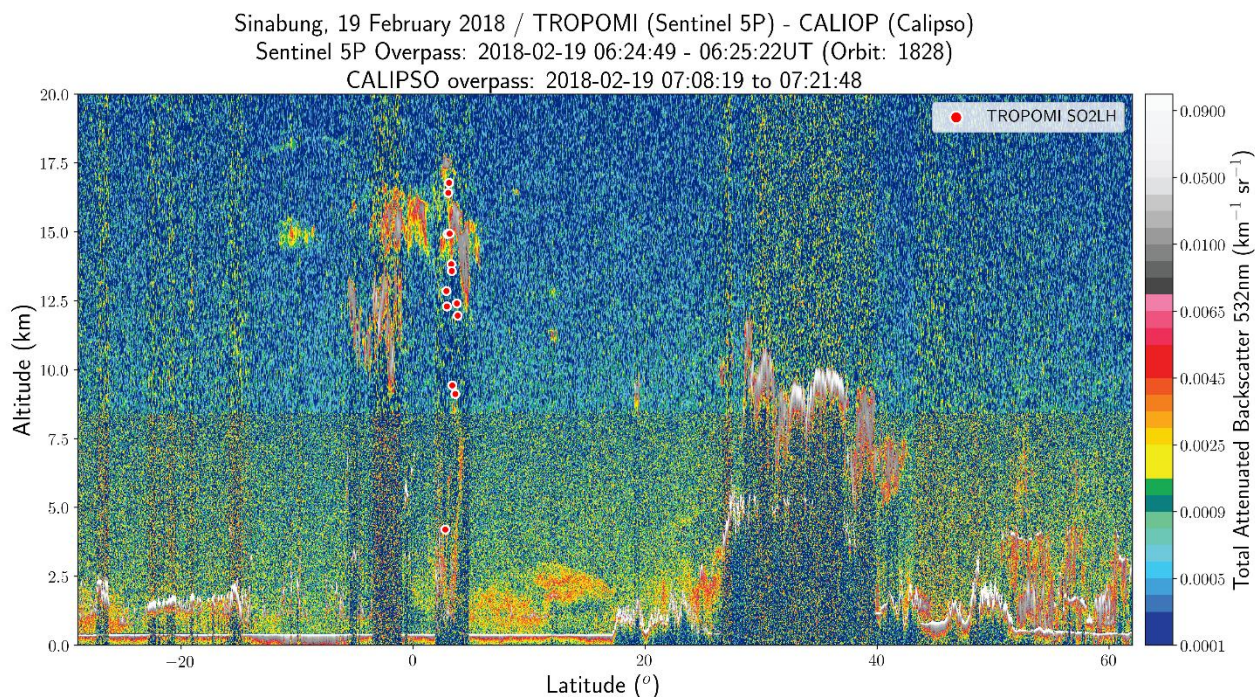


Figure 8. (Left) Scatter plot of the TROPOMI SO₂ LH and CALIPSO weighted height for all collocated pixels on the 22nd, 23rd, 24th, 25th, 28th, 29th and 30th of June 2019, for the Raikoke eruption. (Right) Histogram distribution of the absolute differences between TROPOMI SO₂ LH and the corresponding CALIPSO weighted extinction height measurements, calculated for the 241 collocated points.

405 On the 19th of February 2018, at 08:53 L.T., the Indonesian stratovolcano Mount Sinabung on Sumatra (2460 m summit
 406 elevation) erupted jetting a large ash plume that quickly rose to heights of approximately 15 to 17 km.. Although the eruption
 407 was spatiotemporally small an excellent overpass was found against the CALIPSO instrument (Figure S6, left). The CALIOP
 408 track crossed the main part of the volcanic cloud, across the north-to-south axis. Its overpass time is between 07:08 and
 409 07:22 UTC, a mere 45 min after the TROPOMI overpass time, between 06:24 and 06:26 UTC. The CALIPSO observations
 410 showed both the ash cloud, as a layer around 5 km, as well as two vertical ash clouds extending from the volcano up to ~10 km
 411 altitude. As shown in Figure 9, where the S5P SO₂ LH retrievals are shown in the red dots, the presence of clouds appear along
 412 the CALIPSO path indicated by the stronger attenuated backscatter than the aerosol layer.



413 **Figure 9.** Sinabung, 19th of February 2018, 07:15 UTC. The colours show the CALIOP/CALIPSO total attenuated backscatter
 414 at 532nm and the white-red dots show the TROPOMI SO₂ LH.

415 This case of mixing between ash and clouds over a volcanic eruption renders the retrieval of the ash plume altitude by the lidar
 416 algorithm very difficult, since it cannot separate clouds from aerosols, especially when the aerosol amount is low. The
 417 CALIPSO feature mask (not shown here) hardly identifies any of the Sinabung backscatter signals as aerosol. The main plume,
 418 at ~15 km is flagged a cloud feature, while below this feature everything is masked as “totally attenuated”, which is not

419 expected to be the case. Most probably liquid water or ice particles are contaminating the volcanic ash signal, as already
 420 discussed in Hedelt et al., 2019. Even though the maximum TROPOMI SO₂ LH agrees with the maximum backscatter height
 421 between 2-3° latitude, a large spread of TROPOMI SO₂ LHs are also reported. As discussed also in the work of de Laat et al.,
 422 2020, the presence of either a nearly-transparent or a bright cloud may result in the TROPOMI algorithm reporting heights far
 423 lower than both the ash and the cloud plumes. For the cases of Nishinoshima 2020 and La Soufrière 2021 eruptions, both
 424 provided a satisfactory collocation to the CALIOP orbital path without the difficulties found in the case of Sinabung, 2018,
 425 enabling a meaningful comparison to be made. For Nishinoshima, spatial collocations for the 1st of August 2020 are shown in
 426 Figure S7 (left), while the scatterplot of height values is shown in the right. The geographical collocations between TROPOMI
 427 and CALIOP are not optimal, however the agreement between SO₂ LH and CALIOP weighted extinction altitude is
 428 satisfactory, and tends to confirm the presence of volcanic plumes. The CALIPSO observations confirm the presence of
 429 volcanic clouds around 5 km, while S5P reports slightly higher loads, at ~7.5 km. For the case of La Soufrière, spatial
 430 collocations for the 11st of April 2021 are shown in Figure S8 (left), where the scatterplot of collocations is shown in the right
 431 column and the scatter plots in the right column. In this case, both CALIPSO and TROPOMI collocated pixels confirms the
 432 presence of a volcanic cloud up to and around ~20 km.

433 **4.2.3 Summary of the comparisons with the CALIPSO/CALIOP observations**

434 The combination of CALIOP and TROPOMI data measurements has permitted the identification of volcanic aerosol layers
 435 produced by three individual volcanic eruptions. A summary plot of the comparisons between S5P SO₂ and CALIPSO ash
 436 LHs is presented as a scatter plot in Figure 10, showing the mean ash and SO₂ plume height reported for each of the 9 days of
 437 collocations. The comparison is very promising, with a slope close to 0.95, y-intercept of ~1 km and correlation coefficient of
 438 0.86 for the 9 collocations days for the Raikoke, Nishinoshima and La Soufrière eruptions. The majority of cases, 7 days,
 439 belong to the Raikoke eruptive period, and the remainder 2 days to Nishinoshima and La Soufrière eruptions, respectively.
 440 From Table 4 it is worth noting that the standard deviation of the mean heights reported by both instruments are low, typically
 441 much less than 1 km. This can most likely be attributed to the tight spatiotemporal collocation criteria that were possible for
 442 these comparisons. The behaviour of altitude range differences are also corroborated by the works of Muser et al., 2020; De
 443 Leeuw a et al., 2020 and Osborne et al., 2021: These studies highlight that, for coarse mode ash, the aging process is the
 444 determining factor of the vertical distribution of aerosols and therefore the determining factor for the altitude at which the
 445 particles are transported, apart from meteorology of course.

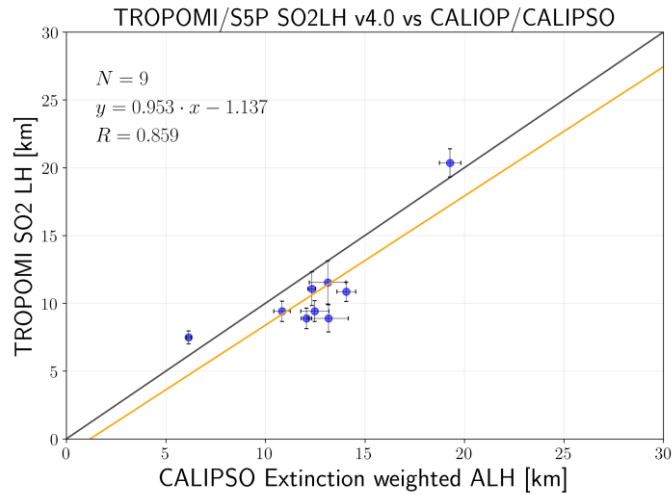


Figure 10. Scatter plot of the mean daily average reported SO₂ LHs by TROPOMI/S5P and CALIOP/CALIPSO for the seven days of the Raikoke eruption and one each for Nishinoshima and La Soufrière eruptions studied.

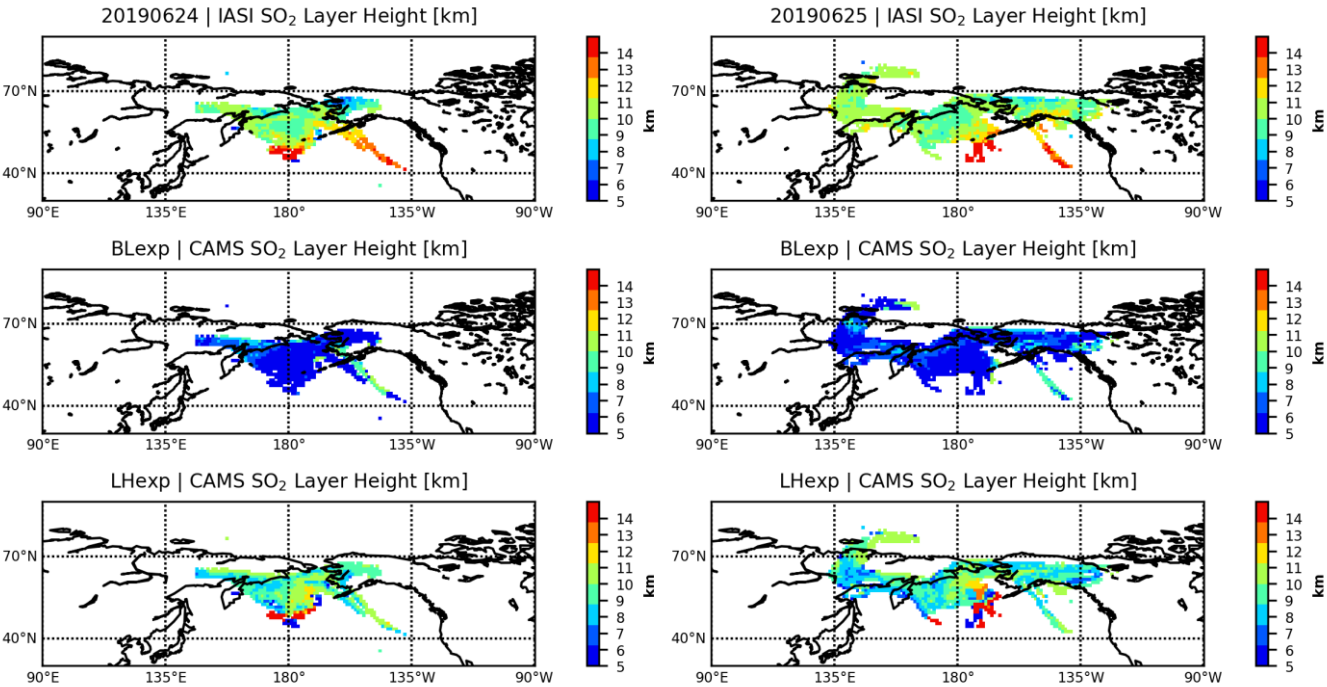
Table 4. Statistics for the comparison between S5P and CALIPSO for the eruptive days studied.

Eruptive day	Mean CALIPSO LH [km]	Mean S5P Height [km]	Mean Difference [km]	Collocations.
22 June 2019	10.84±0.4	9.40±0.75	-1.43±0.56	8
23 June 2019	12.06±0.28	8.88±0.76	-3.17±0.98	13
24 June 2019	12.33±0.2	11.07±1.24	-1.26±1.40	22
25 June 2019	12.47±0.1	9.41±0.76	-3.05±0.54	57
28 June 2019	13.12±0.92	11.53±1.6	-1.59±2.13	87
29 June 2019	14.06±0.47	10.84±0.7	-3.21±0.99	46
30 June 2019	13.16±1	8.88±1	-4.28±0.56	8
01 August 2020	6.14±0.12	7.48±0.48	1.34±0.46	8
11 April 2021	19.28±0.54	20.35±1.04	1.06±1.44	12

Generally, we note that features identified as volcanic ash by the CALIOP aerosol subtype mask are captured by the TROPOMI algorithm, but the surrounding clouds often affect the retrieval. Formation of high-altitude condensed water or ice in the ash plume may shield part of the underlying SO₂ and ash amounts. The comparison of the TROPOMI SO₂ LH product within this project shows promising capability in detecting plumes of volcanic origin, with some limitations related to existing or subsequent creation of clouds. Furthermore, although ash and SO₂ plumes are often collocated especially at the first hours after eruption, this is not always the case, making direct comparisons challenging.

456 **4.3 Application of the S5P SO₂ LH in NRT data assimilation modelling**

457 The Copernicus Atmosphere Monitoring Service (CAMS), operated by the European Centre for Medium-Range Weather
458 Forecasts (ECMWF) on behalf of the European Commission, provides daily SO₂ analyses and 5-day forecasts of volcanic SO₂
459 in NRT by assimilating total column SO₂ retrievals from TROPOMI and GOME-2 (Inness et al., 2022). As the operational
460 NRT TROPOMI and GOME-2 retrievals do not provide any information about the height of the volcanic plumes, the SO₂
461 increments are placed in the mid-troposphere, around 550 hPa (~5 km) in the current operational CAMS configuration.
462



463 **Figure 11.** Raikoke eruptive day of the 24th (left) and 25th (right) of June 2019. Top. The IASI ULB/LATMOS SO₂ layer height in km.
464 Middle. The CAMS BLexp SO₂ layer height (without assimilation). Bottom. The CAMS LHexp SO₂ layer height (with assimilation).

465 The procedure used to assimilate near-real time TROPOMI/S5P and GOME2/Metop SO₂ loads in the operational CAMS NRT
466 data assimilation system was presented, alongside the simultaneous ingestion of the S5P SO₂ LH, Inness et al., 2022. The
467 assimilation was tested for the 2019 Raikoke eruption and was contrasted to the operational CAMS forecasts obtained when
468 assimilating only the TROPOMI SO₂ load. Two example days are shown in this paper to demonstrate how the CAMS
469 assimilation of the S5P SO₂ LH product leads to much improved model output against the non-assimilated IASI layer heights,
470 compared to the original CAMS analysis.

471 In Figure 11, upper, the IASI ULB/LATMOS SO₂ layer height, gridded onto the CAMS 1x1° spatial resolution and 3h temporal
472 resolution, is shown for the 24th (left column) and the 25th (right column) of June 2019, 5 days after the initial Raikoke eruption.

473 In the middle panel, the operational CAMS SO₂ layer height (called BLexp) is presented which is deduced from placing the
 474 SO₂ increment in the mid-troposphere, around 550 hPa, clearly in the wrong altitude for the Raikoke eruption which injected
 475 a huge amount of SO₂ above the tropopause, well into the stratosphere. In Figure 11, lower panel, it can be seen that a vast
 476 improvement to the CAMS forecast is achieved for both days when the S5P SO₂ LH data are used (called LHexp) as the
 477 structure of the Raikoke SO₂ plume is much improved and compares well with the independent IASI SO₂ layer heights shown
 478 in the upper panel. For the entire eruptive period of Raikoke between June 22nd and June 29th, the CAMS forecast which
 479 assimilates the S5P SO₂ LH data improves the bias in the forecast height between CAMS and IASI to $\sim -1.5 \pm 2.5$ km, compared
 480 to a mean bias of $\sim -5 \pm 2$ km for the operational system. We can hence conclude that by assimilating the S5P SO₂ LH data, the
 481 vertical location of the Raikoke SO₂ plume in the CAMS system is improved, leading to better subsequent forecasts and making
 482 the S5P SO₂ LH product suitable for NRT assimilation and forecasts of a possible strong future volcanic eruption.

483 5 Conclusions

484 The European Space Agency Sentinel-5p+ Innovation TROPOMI/S5P SO₂ layer height product has been verified against
 485 IASI/Metop SO₂ layer heights for the eruptive periods of the Raikoke volcano, 22 June to 30 July 2019, the Taal volcano, 13
 486 January 2020, the Nishinoshima eruptive period during July & August 2020 and the La Soufrière eruptive days of April 10th
 487 to 11th, 2021. Two different algorithms that provide plume altitude from the IASI instruments were examined, the official
 488 EUMETSAT ACSAF algorithm, ULB/LATMOS, and the University of Oxford, AOPP, algorithm. Furthermore, collocations
 489 against ash layer height observations by the space-born CALIOP/CALIPSO lidar system were identified and assessed.

490 The main findings in the comparisons of the SO₂ volcanic plumes, described in detail above, are:

- 491 ▪ For the Raikoke eruptive days: the difference between S5P and IASI/AOPP SO₂ LH datasets is 0.61 ± 3.72 km, with
 492 IASI/AOPP SO₂ LH reporting a mean height of $\sim 11.40 \pm 2.5$ km and S5P reporting $\sim 10.75 \pm 3.5$ km, in excellent agreement.
 493 Between S5P and IASI ULB/LATMOS SO₂ LHs a similar mean difference of -0.15 ± 2.83 km is found with both sensors
 494 reporting on average LHs at $\sim 1010.20 \pm 2.80$ km and $\sim 10.00 \pm 1.0$ km respectively.
- 495 ▪ For the Taal eruptive day: the SO₂ LHs reported differ substantially with IASI/AOPP reporting heights at 5.64 ± 1.5 km
 496 while S5P reports higher columns, at $\sim 10.14 \pm 3.5$ km. IASI ULB/LATMOS also reports lower heights, at 9.51 ± 1.78
 497 km while and S5P places the plume at $\sim 12.13 \pm 3.95$ km with a mean difference of $\sim -2.62 \pm 3.0$ km.
- 498 ▪ For the Nishinoshima eruptive days: both sensors place the plume at the same altitude, with IASI ULB/LATMOS at
 499 $\sim 8.0 \pm 1.04$ km and S5P $\sim 7.73 \pm 1.97$ km and mean difference of $\sim 0.27 \pm 2.79$ km.
- 500 ▪ For the La Soufrière eruptive days: all three sensors report high plume altitudes, between 13 and 16 km. For the
 501 collocations between S5P and IASI/AOPP, the mean SO₂ LH was found at 13.82 ± 2.49 km and 13.47 ± 3.41 km
 502 respectively, with a mean difference of -0.35 ± 3.55 km. For the S5P and IASI ULB/LATMOS collocations, the mean SO₂
 503 LH was found at 14.94 ± 3.87 km and 15.7 ± 1.16 km respectively, and a mean difference of 0.76 ± 3.69 km.

504 ▪ Scatter plot comparisons of the daily mean volcanic SO₂ plumes reveal common SO₂ LHs patterns for the two sensors,
505 with substantial correlations ~0.66 (0.72), slope ~0.9 (0.98), y-intercept of 1.2 km (0.8 km) for the IASI/AOPP and the
506 IASI ULB/LATMOS respectively. The standard deviation of the mean is relatively high, on average ~3 km, however the
507 mean heights are well within the 2 km accuracy requirement on the S5P SO₂ layer height product.

508 With respect to the comparisons between the S5P SO₂ LH and the CALIOP/CALIPSO volcanic ash layer height, we report
509 that:

510 ▪ 241 excellently spatiotemporally collocated points between CALIOP and TROPOMI were identified for seven Raikoke
511 eruptive days. CALIOP reported a range of mean heights between ~11 and 14 km, while TROPOMI had a far narrower
512 range between ~9 and 11.5 km. Overall, the mean difference in heights was found to be -2.4±1.7 km (-3.0 km median) for
513 the seven eruptive Raikoke days.

514 ▪ The comparisons for the Nishinoshima and La Soufrière eruptions showed good agreement with plumes reported at ~7
515 km (~19.5 km) respectively for the two eruptions, and a height difference between S5P and CALIPSO being within ~1.0
516 km.

517 ▪ The mean daily height comparative plot of the comparisons between S5P SO₂ LHs and CALIOP/CALIPSO weighted
518 ALH, as expected, follow a straight line, with slope of 0.95 and y-intercept of ~1.0 km and excellent correlation coefficient
519 at 0.86.

520 Finally, the CAMS assimilation of the NRT S5P SO₂ LH led to much improved model fields against the non-assimilated IASI
521 plume heights for the Raikoke eruptive period, with a mean difference of 1.5±2 km against the independent IASI/Metop
522 observations, and improved the geographical spread of the Raikoke volcanic plume following the main eruptive day.

523

524 **Data availability.** The near-real-time S5P SO₂ LH products are operationally generated by DLR in the framework of the
525 Innovative Products for Analyses of Atmospheric Composition, INPULS, project, and are available upon request from
526 Pascal Hedelt (Pascal.Hedelt@dlr.de). The IASI/MetOp ULB/LATMOS open source SO₂ layer height dataset is publicly
527 available from https://iasi.aeris-data.fr/so2_iasi_a_arch/ (last access: 20.07.2021). The IASI/MetOp AOPP SO₂ products are
528 available on request from Isabelle Taylor (isabelle.taylor@physics.ox.ac.uk). The CALIPSO data were obtained from the
529 online archive of the NASA Langley Research Center Atmospheric Science Data Center (ASDC,
530 <https://asdc.larc.nasa.gov/project/CALIPSO>). The Copernicus Atmosphere Monitoring Service is operated by the European
531 Centre for Medium-Range Weather Forecasts on behalf of the European Commission as part of the Copernicus program
532 (<http://copernicus.eu>) and CAMS data are freely available from atmosphere.copernicus.eu/data. The SO₂ analysis
533 experiments used in this paper are available from <https://apps.ecmwf.int/research-experiments/expver/> with the DOIs:
534 10.21957/cygt-xf49 (BLexp), 10.21957/qfam-7474 (LHexp).

535

536 **Acknowledgments** This work is performed in the framework of ESA's Sentinel-5p+ Innovation: SO₂ Layer Height project
537 (S5P+I: SO2LH), <https://eo4society.esa.int/projects/sentinel-5p-innovation-so2-layer-height-project/>. The comparative results

presented in this work have been produced using the Aristotle University of Thessaloniki High Performance Computing Infrastructure and Resources. M.E.K. would like to acknowledge the support provided by the IT Center of the Aristotle University of Thessaloniki throughout the progress of this research work, as well as the Atmospheric Toolbox®. I.A.T. and R.G.G. would like to acknowledge EUMETSAT for providing the IASI spectra and ECMWF and CEDA for the meteorological profiles used in the IASI retrievals. I.A.T. and R.G.G. further acknowledge support from the NERC Centre for Observation and Modelling of Earthquakes, Volcanoes, and Tectonics (COMET). We thank the DLR Innovative Products for Analyses of Atmospheric Composition (INPULS) project, for continuously providing the S5P SO₂ LH products in near-real-time.

References

- Ahn S, Jee J-B, Lee K-T, Oh H-J. Enhanced Accuracy of Airborne Volcanic Ash Detection Using the GEOKOMPSAT-2A Satellite. *Sensors*. 2021; 21(4):1359. <https://doi.org/10.3390/s21041359>.
- Astoreca R., D. Hurtmans, L. Clarisse, P. Coheur, M. George, J. Hadji-Lazaro and C. Clerbaux, ACSAF Product User Manual for the Near real-time IASI Brescia SO₂ product, SAF/AC/ULB/PUM/002, v1.2, 2018.
- Balis, D., M. E. Koukouli, Siomos, N., et al., Validation of ash optical depth and layer height retrieved from passive satellite sensors using EARLINET and airborne lidar data: The case of the Eyjafjallajökull eruption, *Atmospheric Chemistry and Physics*, <http://dx.doi.org/10.5194/acp-16-5705-2016>, 2016.
- Boichu, M., Clarisse, L., Péré, J.-C., Herbin, H., Goloub, P., Thieuleux, F., Ducos, F., Clerbaux, C., and Tanré, D.: Temporal variations of flux and altitude of sulfur dioxide emissions during volcanic eruptions: implications for long-range dispersal of volcanic clouds, *Atmos. Chem. Phys.*, 15, 8381–8400, <https://doi.org/10.5194/acp-15-8381-2015>, 2015.
- Bolić T, Sivčev Ž. Eruption of Eyjafjallajökull in Iceland: Experience of European Air Traffic Management. *Transportation Research Record*. 2011;2214(1):136-143. doi:10.3141/2214-17
- Brenot, H., Theys, N., Clarisse, L., van Geffen, J., van Gent, J., Van Roozendaal, M., van der A, R., Hurtmans, D., Coheur, P.-F., Clerbaux, C., Valks, P., Hedelt, P., Prata, F., Rason, O., Sievers, K., and Zehner, C.: Support to Aviation Control Service (SACS): an online service for near-real-time satellite monitoring of volcanic plumes, *Nat. Hazards Earth Syst. Sci.*, 14, 1099–1123, <https://doi.org/10.5194/nhess-14-1099-2014>, 2014.
- Brenot, H., Theys, N., Clarisse, L., van Gent, J., Hurtmans, D. R., Vandenbussche, S., Papagiannopoulos, N., Mona, L., Virtanen, T., Uppstu, A., Sofiev, M., Bugliaro, L., Vázquez-Navarro, M., Hedelt, P., Parks, M. M., Barsotti, S., Coltelli, M., Moreland, W., Scollo, S., Salerno, G., Arnold-Arias, D., Hirtl, M., Peltonen, T., Lahtinen, J., Sievers, K., Lipok, F., Rüfenacht, R., Haeferle, A., Hervé, M., Wagenaar, S., Som de Cerff, W., de Laat, J., Apituley, A., Stammes, P., Laffineur, Q., Delcloo, A., Lennart, R., Rokitansky, C.-H., Vargas, A., Kerschbaum, M., Resch, C., Zopp, R., Plu, M., Peuch, V.-H., Van Roozendaal, M., and Wotawa, G.: EUNADICS-AV early warning system dedicated to supporting aviation in the case of a crisis from natural airborne hazards and radionuclide clouds, *Nat. Hazards Earth Syst. Sci.*, 21, 3367–3405, <https://doi.org/10.5194/nhess-21-3367-2021>, 2021.

570 Campbell, J. R., Tackett, J. L., Reid, J. S., Zhang, J., Curtis, C.A., Hyer, E. J., Sessions, W. R., Westphal, D. L., Prospero,
571 J.M., Welton, E. J., Omar, A. H., Vaughan, M. A., and Winker, D. M.: Evaluating nighttime CALIOP 0.532 μm aerosol
572 optical depth and extinction coefficient retrievals, *Atmos. Meas. Tech.*, 5, 2143–2160, [https://doi.org/10.5194/amt-5-2143-](https://doi.org/10.5194/amt-5-2143-2012)
573 2012, 2012.

574 Carboni, E., Grainger, R., Walker, J., Dudhia, A., and Siddans, R.: A new scheme for sulphur dioxide retrieval from IASI
575 measurements: application to the Eyjafjallajökull eruption of April and May 2010, *Atmos. Chem. Phys.*, 12, 11417–11434,
576 <https://doi.org/10.5194/acp-12-11417-2012>, 2012.

577 Carboni, E., R.G. Grainger, T.A. Mather, D.M. Pyle G.E. Thomas, R. Siddans, A.J.A. Smith, A. Dudhia, M.E. Koukouli and
578 D. Balis, The vertical distribution of volcanic SO_2 plumes measured by IASI, *Atmospheric Chemistry and Physics*, 16,
579 4343–4367, 2016. (doi:10.5194/acp-16-4343-2016)

580 Carn, S. A., K. Yang, A. J. Prata and N. A. Krotkov, Extending the long-term record of volcanic SO_2 emissions with the Ozone
581 Mapping and Profiler Suite (OMPS) Nadir Mapper, *Geophys. Res. Lett.*, 42, 925-932, doi:10.1002/2014GL062437, 2015.

582 Carn, S. A., L. Clarisse, A.J. Prata, Multi-decadal satellite measurements of global volcanic degassing, *Journal of Volcanology*
583 and *Geothermal Research*, 311, 99-134, ISSN 0377-0273, <https://doi.org/10.1016/j.jvolgeores.2016.01.002>, 2016.

584 Clarisse, L., Coheur, P.-F., Theys, N., Hurtmans, D., and Clerbaux, C.: The 2011 Nabro eruption, a SO_2 layer height analysis
585 using IASI measurements, *Atmos. Chem. Phys.*, 14, 3095-3111, <https://doi.org/10.5194/acp-14-3095-2014>, 2014.

586 Clarisse, L., Hurtmans, D., Clerbaux, C., Hadji-Lazaro, J., Ngadi, Y., and Coheur, P.-F.: Retrieval of sulphur dioxide from the
587 infrared atmospheric sounding interferometer (IASI), *Atmos. Meas. Tech.*, 5, 581-594, doi:10.5194/amt-5-581-2012, 2012.

588 de Laat, A., Vazquez-Navarro, M., Theys, N., and Stammes, P.: Analysis of properties of the 19 February 2018 volcanic
589 eruption of Mount Sinabung in TROPOMI/S5P and Himawari-8 satellite data, *Nat. Hazards Earth Syst. Sci.*, 20, 1203–
590 1217, <https://doi.org/10.5194/nhess-20-1203-2020>, 2020.

591 de Leeuw, J., Schmidt, A., Witham, C. S., Theys, N., Taylor, I. A., Grainger, R. G., Pope, R. J., Haywood, J., Osborne, M.,
592 and Kristiansen, N. I.: The 2019 Raikoke volcanic eruption – Part 1: Dispersion model simulations and satellite retrievals
593 of volcanic sulfur dioxide, *Atmos. Chem. Phys.*, 21, 10851–10879, <https://doi.org/10.5194/acp-21-10851-2021>, 2021.

594 Eckhardt, S., Prata, A. J., Seibert, P., Stebel, K., and Stohl, A.: Estimation of the vertical profile of sulfur dioxide injection into
595 the atmosphere by a volcanic eruption using satellite column measurements and inverse transport modeling, *Atmos. Chem.*
596 *Phys.*, 8, 3881–3897, <https://doi.org/10.5194/acp-8-3881-2008>, 2008.

597 Efremenko, D.S., Loyola, D.G.R., Hedelt, P., and Spurr, R.J.D. Volcanic SO_2 plume height retrieval from UV sensors using a
598 full-physics inverse learning machine algorithm, *International Journal of Remote Sensing*, 38, sup1, 1-27, doi:
599 10.1080/01431161.2017.1348644, 2017

600 European Centre for Medium-Range Weather Forecasts (2012): ECMWF Operational Regular Gridded Data at 1.125 degrees
601 resolution. NCAS British Atmospheric Data Centre, 12th July 2021.
602 <https://catalogue.ceda.ac.uk/uuid/a67f1b4d9db7b1528b800ed48198bdac>

603 Fedkin, N. M., Li, C., Krotkov, N. A., Hedelt, P., Loyola, D. G., Dickerson, R. R., and Spurr, R.: Volcanic SO₂ effective layer
604 height retrieval for the Ozone Monitoring Instrument (OMI) using a machine-learning approach, *Atmos. Meas. Tech.*, 14,
605 3673–3691, <https://doi.org/10.5194/amt-14-3673-2021>, 2021.

606 Hedelt, P. and Koukouli, M. E.: S5p+I - SO₂ Layer Height Algorithm Theoretical Baseline Document (ATBD),
607 <https://doi.org/10.5281/zenodo.5118540>, 2021.

608 Hedelt, P., Efremenko, D. S., Loyola, D. G., Spurr, R., and Clarisse, L.: Sulfur dioxide layer height retrieval from Sentinel-5
609 Precursor/TROPOMI using FP_ILM, *Atmos. Meas. Tech.*, 12, 5503–5517, <https://doi.org/10.5194/amt-12-5503-2019>,
610 2019.

611 Hughes, E. J., Sparling, L. C., Carn, S. A., and Krueger, A. J.(2012), Using horizontal transport characteristics to infer an
612 emission height time series of volcanic SO₂, *J. Geophys. Res.*, 117, D18307, doi:[10.1029/2012JD017957](https://doi.org/10.1029/2012JD017957).

613 Hyman, D. M. and Pavolonis, M. J.: Probabilistic retrieval of volcanic SO₂ layer height and partial column density using the
614 Cross-track Infrared Sounder (CrIS), *Atmos. Meas. Tech.*, 13, 5891–5921, <https://doi.org/10.5194/amt-13-5891-2020>,
615 2020.

616 ICAO: International Civil Aviation Organization, Flight Safety and Volcanic Ash, Roadmap for International Airways
617 Volcano Watch (IAVW) in Support of International Air Navigation, 18.11.2019, v 4.0,
618 [https://www.icao.int/airnavigation/METP/MOGVA Reference Documents/IAVW Roadmap.pdf](https://www.icao.int/airnavigation/METP/MOGVA/Reference%20Documents/IAVW%20Roadmap.pdf), last access: 19.01.2022,
619 2019.

620 Inness, A., Ades, M., Balis, D., Efremenko, D., Flemming, J., Hedelt, P., Koukouli, M.-E., Loyola, D., and Ribas, R.:
621 Evaluating the assimilation of S5P/TROPOMI near real-time SO₂ columns and layer height data into the CAMS integrated
622 forecasting system (CY47R1), based on a case study of the 2019 Raikoke eruption, *Geosci. Model Dev.*, 15, 971–994,
623 <https://doi.org/10.5194/gmd-15-971-2022>, 2022..

624 Jing F, Chauhan A, P Singh R, Dash P. Changes in Atmospheric, Meteorological, and Ocean Parameters Associated with the
625 12 January 2020 Taal Volcanic Eruption. *Remote Sensing*. 2020; 12(6):1026. <https://doi.org/10.3390/rs12061026>.

626 Kim, M.-H., Omar, A. H., Tackett, J. L., Vaughan, M. A., Winker, D. M., Trepte, C. R., Hu, Y., Liu, Z., Poole, L. R., Pitts, M.
627 C., Kar, J., and Magill, B. E.: The CALIPSO version 4 automated aerosol classification and lidar ratio selection algorithm,
628 *Atmos. Meas. Tech.*, 11, 6107–6135, <https://doi.org/10.5194/amt-11-6107-2018>, 2018.

629 Kloss, C., Berthet, G., Sellitto, P., Ploeger, F., Taha, G., Tidiga, M., Eremenko, M., Bossolasco, A., Jégou, F., Renard, J.-B.,
630 and Legras, B.: Stratospheric aerosol layer perturbation caused by the 2019 Raikoke and Ulawun eruptions and their
631 radiative forcing, *Atmos. Chem. Phys.*, 21, 535–560, <https://doi.org/10.5194/acp-21-535-2021>, 2021.

632 Koffi, B., Schulz, M., Bréon, F.-M., Griesfeller, J., Winker, D., Balkanski, Y., Bauer, S., Bernsten, T., Chin, M., Collins, W.
633 D., Dentener, F., Diehl, T., Easter, R., Ghan, S., Ginoux, P., Gong, S., Horowitz, L. W., Iversen, T., Kirkevåg, A., Koch,
634 D., Krol, M., Myhre, G., Stier, P., and Takemura, T.: Application of the CALIOP layer product to evaluate the vertical
635 distribution of aerosols estimated by global models: AeroCom phase I results, *J. Geophys. Res.-Atmos.*, 117, D10,
636 <https://doi.org/10.1029/2011JD016858>, 2012.

637 Koukouli, M. E., Balis, D., Michailidis, K, Hedelt, P.: S5p+I - SO₂ Layer Height Validation Report (VR),
638 <https://doi.org/10.5281/zenodo.5118558>, 2021.

639 Koukouli, M.E, D. Balis, S. Dimopoulos, & N. Siomos, SACS-2/SMASH – Validation Report on the Eyjafjallajökull and
640 Grimsvötn eruptions (v1.0). Zenodo. <https://doi.org/10.5281/zenodo.5566654>, 2014.

641 Liu, D., Wang, Z., Liu, Z., Winker, D., and Trepte, C. (2008), A height resolved global view of dust aerosols from the first
642 year CALIPSO lidar measurements, *J. Geophys. Res.*, 113, D16214, doi:10.1029/2007JD009776.

643 Lopes, F. J. S., Silva, J.J., Antuña Marrero, J.C., Taha, G. and Landulfo, E., Synergetic Aerosol Layer Observation after the
644 2015 Calbuco Volcanic Eruption Event. *Remote Sens.*, 11, 195. <https://doi.org/10.3390/rs11020195>, 2019.

645 Loyola, D. G., Pedernana, M., and Gimeno Garcia, S., Smart sampling and incremental function learning for very large high
646 dimensional data. *Neural Networks*, <https://doi.org/10.1016/j.neunet.2015.09.001>, 78:75–87, 2016.

647 Loyola, D. G., Xu, J., Heue, K.-P., and Zimmer, W.: Applying FP_ILM to the retrieval of geometry-dependent effective
648 Lambertian equivalent reflectivity (GE_LER) daily maps from UVN satellite measurements, *Atmos. Meas. Tech.*, 13, 985–
649 999, <https://doi.org/10.5194/amt-13-985-2020>, 2020.

650 McKee, Kathleen, Cassandra M. Smith, Kevin Reath, Eveanjelene Snee, Sean Maher, Robin S. Matoza, Simon Carn, Larry
651 Mastin, Kyle Anderson, David Damby, Diana C. Roman, Artem Degterev, Alexander Rybin, Marina Chibisova, Jelle D.
652 Assink, Rodrigo de Negri Leiva, Anna Perttu, Evaluating the state-of-the-art in remote volcanic eruption characterization
653 Part I: Raikoke volcano, Kuril Islands, *Journal of Volcanology and Geothermal Research*, Volume 419, 107354, ISSN
654 0377-0273, <https://doi.org/10.1016/j.jvolgeores.2021.107354>, 2021.

655 Muser, L. O., Hoshyaripour, G. A., Bruckert, J., Horváth, Á., Malinina, E., Wallis, S., Prata, F. J., Rozanov, A., von Savigny,
656 C., Vogel, H., and Vogel, B.: Particle aging and aerosol–radiation interaction affect volcanic plume dispersion: evidence
657 from the Raikoke 2019 eruption, *Atmos. Chem. Phys.*, 20, 15015–15036, <https://doi.org/10.5194/acp-20-15015-2020>,
658 2020.

659 Nanda, S., de Graaf, M., Veefkind, J. P., Sneep, M., ter Linden, M., Sun, J., and Levelt, P. F.: A first comparison of TROPOMI
660 aerosol layer height (ALH) to CALIOP data, *Atmos. Meas. Tech.*, 13, 3043–3059, [https://doi.org/10.5194/amt-13-3043-](https://doi.org/10.5194/amt-13-3043-2020)
661 2020, 2020.

662 Omar, A., Winker, D., Kittaka, C., Vaughan, M., Liu, Z., Hu, Y. X., Trepte, C., Rogers, R., Ferrare, R., Lee, K., Kuehn, R.,
663 and Hostetler, C.: The CALIPSO automated aerosol classification and lidar ratio selection algorithm, *J. Atmos. Ocean.*
664 *Tech.*, 26,1994–2014, doi:10.1175/2009jtecha1231.1, 2009.

665 Osborne, M. J., de Leeuw, J., Witham, C., Schmidt, A., Beckett, F., Kristiansen, N., Buxmann, J., Saint, C., Welton, E. J.,
666 Fochesatto, J., Gomes, A. R., Bundke, U., Petzold, A., Marengo, F., and Haywood, J.: The 2019 Raikoke volcanic eruption
667 part 2: Particle phase dispersion and concurrent wildfire smoke emissions, *Atmos. Chem. Phys. Discuss.* [preprint],
668 <https://doi.org/10.5194/acp-2021-448>, in review, 2021.

669 Pardini, Federica, Mike Burton, Fabio Arzilli, Giuseppe La Spina, Margherita Polacci, SO₂ emissions, plume heights and
 670 magmatic processes inferred from satellite data: The 2015 Calbuco eruptions, *Journal of Volcanology and Geothermal*
 671 *Research*, Volume 361, 2018, Pages 12-24, ISSN 0377-0273, <https://doi.org/10.1016/j.jvolgeores.2018.08.001>, 2018.

672 Perttu, Anna, Benoit Taisne, Silvio De Angelis, Jelle D. Assink, Dorianne Tailpied, Ross Adrian Williams, Estimates of plume
 673 height from infrasound for regional volcano monitoring, *Journal of Volcanology and Geothermal Research*, 402, 106997,
 674 ISSN 0377-0273, <https://doi.org/10.1016/j.jvolgeores.2020.106997>, 2020.

675 Prata, A. T., Young, S. A., Siems, S. T., and Manton, M. J.: Lidar ratios of stratospheric volcanic ash and sulfate aerosols
 676 retrieved from CALIOP measurements, *Atmos. Chem. Phys.*, 17, 8599–8618, <https://doi.org/10.5194/acp-17-8599-2017>,
 677 2017.

678 Prata, A.J. Satellite detection of hazardous volcanic clouds and the risk to global air traffic. *Nat Hazards* **51**, 303–324 (2009).
 679 <https://doi.org/10.1007/s11069-008-9273-z>

680 Rajapakshe, C., Zhang, Z., Yorks, J. E., Yu, H., Tan, Q., Meyer, K., Platnick, S., and Winker, D. M.: Seasonally transported
 681 aerosol layers over southeast Atlantic are closer to underlying clouds than previously reported, *Geophys. Res. Lett.*, 44,
 682 5818–5825, <https://doi.org/10.1002/2017GL073559>, 2017.

683 Reichardt U, Ulfarsson GF, Petursdottir G. Cooperation Between Science and Aviation-Sector Service Providers in Europe
 684 for Risk Management of Volcanic Ash. *Transportation Research Record*. 2017;2626(1):99-105. doi:10.3141/2626-12

685 Saunders, R. W., Matricardi, M., and Brunel, P.: An improved fast radiative transfer model for assimilation of satellite radiance
 686 observations, *Q. J. Roy. Meteor. Soc.*, 125, 1407-1425, <https://doi.org/10.1002/qj.1999.49712555615>, 1999

687 Tournigand, P-Y, Valeria Cigala, Alfredo J. Prata, Andrea K. Steiner, Gottfried Kirchengast, Hugues Brenot, Lieven Clarisse
 688 and Riccardo Biondi, The 2015 Calbuco Volcanic Cloud Detection Using GNSS Radio Occultation and Satellite Lidar,
 689 IGARSS 2020 - 2020 IEEE International Geoscience and Remote Sensing Symposium, 2020, pp. 6834-6837, doi:
 690 10.1109/IGARSS39084.2020.9323356

691 Vaughan, M., Pitts, M., Trepte, C., Winker, D., Detweiler, P., Garnier, A., Getzewich, B., Hunt, W., Lambeth, J., Lee, K.-P.,
 692 Lucker, P., Murray, T., Rodier, S., Tremas, T., Bazureau, A., and Pelon, J.: Cloud-Aerosol LIDAR Infrared Pathfinder
 693 Satellite Observations (CALIPSO) data management system data products catalog, Release 4.92, NASA Langley Research
 694 Center Document PC-SCI-503, available at: https://www-calipso.larc.nasa.gov/products/CALIPSO_DPC_Rev4x92.pdf,
 695 last access: 14 September 2020, 225 pp., 2020.

696 Vira, J., E. Carboni, R. G. Grainger and M. Sofiev, Variational assimilation of IASI SO₂ layer height and total column retrievals
 697 in the 2010 eruption of Eyjafjallajökull using the SILAM v5.3 chemistry transport model, *Geosci. Model Dev.*, 10, 1985-
 698 2008, doi:10.5194/gmd-10-1985-2017, 2017.

699 Walker, J. C., Dudhia, A., and Carboni, E.: An effective method for the detection of trace species demonstrated using the
 700 MetOp Infrared Atmospheric Sounding Interferometer, *Atmos. Meas. Tech.*, 4, 1567–1580, [https://doi.org/10.5194/amt-4-](https://doi.org/10.5194/amt-4-1567-2011)
 701 1567-2011, 2011.

- Walker, J.C., E. Carboni, A. Dudhia and R.G. Grainger, Improved detection of sulphur dioxide in volcanic plumes using satellite-based hyperspectral infrared measurements: Application to the Eyjafjallajökull 2010 eruption, *Journal of Geophysical Research*, 117, D00U16, <https://doi.org/10.1029/2011JD016810>, 2012.
- Wang, J., S. Park, J. Zeng, K. Yang, S. Carn, N. Krotkov, and A. H. Omar, Modeling of 2008 Kasatochi volcanic sulphate direct radiative forcing: assimilation of OMI SO₂ layer height data and comparison with MODIS and CALIOP observations, *Atmos. Chem. Phys.*, 13, 1895-1912, doi:10.5194/acp-13-1895-2013, 2012.
- Winker, D. M., Tackett, J. L., Getzewich, B. J., Liu, Z., Vaughan, M. A., and Rogers, R. R.: The global 3-D distribution of tropospheric aerosols as characterized by CALIOP, *Atmos. Chem. Phys.*, 13, 3345–3361, <https://doi.org/10.5194/acp-13-3345-2013>, 2013.
- Winker, D. M., Z. Liu, A. Omar, J. Tackett, and D. Fairlie, CALIOP observations of the transport of ash from the Eyjafjallajökull volcano in April 2010, *J. Geophys. Res.*, 117, D00U15, doi:10.1029/2011JD016499, 2012.
- Winker, D., Pelon, J., Coakley, J., Ackerman, S., Charlson, R., Colarco, P., Flamant, P., Fu, Q., Hoff, R., Kittaka, C., Kubar, T., Le Treut, H., McCormick, M., Megie, G., Poole, L., Powell, K., Trepte, C., Vaughan, M., and Wielicki, B.: The CALIPSO Mission: a global 3-D view of aerosols and clouds, *B. Am. Meteorol. Soc.*, 91, 1211–1229, <https://doi.org/10.1175/2010BAMS3009.1>, 2010.
- Xu, J., Schüssler, O., Loyola Rodriguez, D. G., Romahn, F., and Doicu, A.: A novel ozone profile shape retrieval using Full-Physics Inverse Learning Machine (FP_ILM), *IEEE J. Sel. Topics Appl. Earth Observ. Remote Sens.*, 10, 5442–5457, <https://doi.org/10.1109/JSTARS.2017.2740168>, 2017.
- Zehner, C., Ed. (2012). Monitoring Volcanic Ash from Space. ESA–EUMETSAT workshop on the 14 April to 23 May 2010 eruption at the Eyjafjöll volcano, South Iceland (ESA/ESRIN, 26–27 May 2010) ESA Publication STM-280. doi:10.5270/atmch-10-01.